

# Energy Distribution Analysis in Boosted HCCI-like / LTGC Engines – Understanding the Trade-offs to Maximize the Thermal Efficiency

Jeremie Dernette, John E. Dec and Chunsheng Ji

Sandia National Laboratories

## Abstract

A detailed understanding of the various factors affecting the trends in gross-indicated thermal efficiency with changes in key operating parameters has been carried out, applied to a one-liter displacement single-cylinder boosted Low-Temperature Gasoline Combustion (LTGC) engine. This work systematically investigates how the supplied fuel energy splits into the following four energy pathways: gross-indicated thermal efficiency, combustion inefficiency, heat transfer and exhaust losses, and how this split changes with operating conditions. Additional analysis is performed to determine the influence of variations in the ratio of specific heat capacities ( $\gamma$ ) and the effective expansion ratio, related to the combustion-phasing retard (CA50), on the energy split. Heat transfer and exhaust losses are computed using multiple standard cycle analysis techniques. The various methods are evaluated in order to validate the trends.

This work focuses on explaining the trends in thermal efficiency and the various energy-loss terms for independent sweeps of fueling rate, intake temperature and engine speed. Trends in thermal efficiency can be well-explained by considering variations in combustion efficiency, CA50 retard,  $\gamma$  and heat transfer. By identifying the energy losses, these results provide a new understanding that can help to optimize the thermal efficiency across the load/speed range in LTGC engines. Of particular importance, a picture is provided of how the heat transfer varies with changes in engine operating conditions. For example, results indicate that CA50 and the magnitude of the acoustic oscillations (*i.e.* knock) are fundamental parameters affecting the heat transfer.

## Introduction

Current engine research is largely oriented toward improving the overall thermal efficiency while meeting stringent emissions regulations and maintaining acceptable combustion noise levels. Toward this goal, engines utilizing Low-Temperature Gasoline Combustion (LTGC), including Homogeneous Charge Compression Ignition (HCCI) and partially stratified variations of HCCI, are attractive because of their superior fuel efficiency, particularly compared to conventional Spark Ignition (SI) engines but also to the latest generations of emissions-compliant Diesel engines [1, 2].

Because the charge in an LTGC engine is sufficiently well-mixed and globally lean or dilute (typically  $\phi_m < 0.5$ <sup>1</sup>), combustion temperatures are low, and NO<sub>x</sub> and soot formation zones are essentially avoided [2, 3]. This eliminates the need for the costly aftertreatment systems for soot and NO<sub>x</sub>. Expensive high-pressure and fast-response fuel-injection technology is also not required for in-cylinder pollutant management. Thus, in LTGC engines, thermal efficiency is not compromised to minimize NO<sub>x</sub> and particulate emissions. Without this constraint, a higher potential exists to finely optimize the control parameters to always provide the highest efficiency.

Peak gross-indicated thermal efficiencies ( $\eta_{th}$ )<sup>2</sup> as high as 48.3% have been previously reported for the mid-size (one-liter displacement) boosted-LTGC engine used in this study with a 14:1 Compression Ratio (CR) [4]. The results of the present study report a peak- $\eta_{th}$  of 49.4% for this same engine using a CR = 16:1.  $\eta_{th}$  above 50% have also been achieved using a larger engine size with a higher CR [5]. It is of interest to further extend the  $\eta_{th}$  for a given engine geometry in order to demonstrate the full potential of boosted-LTGC engines. Perhaps more important is to maintain high efficiencies across the load/speed range of the engine. To achieve these goals, it is necessary to understand in detail the factors affecting the  $\eta_{th}$  and how their contributions vary with changes in the engine operating parameters. There are three main factors that affect the  $\eta_{th}$  [2, 4, 6]: 1) the combustion efficiency ( $\eta_{comb}$ ), 2) the thermodynamic efficiency and 3) the wall Heat Transfer (HT)<sup>3</sup>. These factors are affected by several sub-effects that tradeoff differently depending on the operating parameter that is varied.

In LTGC engines,  $\eta_{comb}$  is an important factor affecting the  $\eta_{th}$  for low loads, or more correctly low- $\phi_m$  [2, 4]. A peak-charge temperature above 1500 K is required to prevent incomplete bulk-gas CO-to-CO<sub>2</sub> reactions [2, 7-10]. Below this temperature, the  $\eta_{comb}$

<sup>1</sup>  $\phi_m$ : charge-mass equivalence ratio as introduced with Equation 2.

<sup>2</sup> Since this study focuses on combustion-related phenomena in a single-cylinder research engine, gross-indicated thermal efficiencies, denoted as  $\eta_{th}$ , are used rather than brake or net thermal efficiencies, as explained in greater detail in the Experimental Setup section.  $\eta_{th}$  will be defined with Equation 4.

<sup>3</sup> In practice, the blow-by losses also affect the  $\eta_{th}$  through losses of pressure and fuel mass. In the analysis conducted in this study, its contribution was not considered. Blow-by was measured in our engine for a range of conditions and was found to be minimal. For instance, a change in boost pressure from 1 to 2 bar increases the blow-by from 0.28 to 0.30% of the total mass. Blow-by losses decrease by 0.41% for an increase in engine speed from 600 to 1800 RPM. Since the change in measured  $\eta_{th}$  will be about half of the variation in the loss of mass, this effect in the noise of the  $\eta_{th}$  measurements and can reasonably be neglected.

drops off quickly and the  $\eta_{th}$  is severely deteriorated [8]. Above this temperature, the  $\eta_{comb}$  is generally relatively high (above ~96%), and the main sources of HC and CO are incomplete combustion of gases in or out-gazing from the top-land crevice and mixture near the walls [11, 12]. For higher load conditions, higher thermal environment still favors oxidation and higher  $\eta_{comb}$  [13]. However, the increasing rate of  $\eta_{comb}$  is much lower and for these relatively high- $\eta_{comb}$  conditions,  $\eta_{comb}$  was found to not be any longer a decisive factor influencing the variations in  $\eta_{th}$  (change in  $\eta_{comb}$  too small) [4]. Also, the need to use Exhaust Gas Recirculation (EGR)<sup>4</sup> helps improve  $\eta_{comb}$  by providing a second chance for the HC and CO in the EGR to burn [13].

As given by the theoretical equation for isentropic compression/expansion (Equation 1), the thermodynamic efficiency depends on two parameters: CR and  $\gamma$ , the ratio of specific heats ( $c_p/c_v$ ). The higher the CR or  $\gamma$ , the higher the thermodynamic efficiency, leading to more work extracted and less energy lost into the exhaust gases.

$$\eta_{thermodynamic} = 1 - \frac{1}{CR^{\gamma} - 1} \quad (1)$$

For a given engine geometry, CA50 affects the effective expansion ratio and thus the thermodynamic efficiency: retarding the CA50 after Top Dead Center (TDC) lowers the expansion efficiency [2, 4, 6]. Alternatively, to maximize the thermodynamic efficiency, it is desirable to advance as much as possible toward TDC, while considering the CA50 limitation imposed by the need to avoid excessive combustion noise/knock [2, 14]. However, as shown by Dec *et al.* [4], for relatively high  $\eta_{comb}$  conditions, there is little potential benefit to advancing CA50 beyond about 366-368°CA, even without knock, since the piston motion per Crank Angle (CA) degree is small near TDC, and HT losses increases, as discussed below.

$\gamma$ , is sensitive to the charge composition and temperature:  $\gamma$  decreases with higher cycle temperatures, and with higher EGR and  $\phi_m$  (more tri-atomic molecules). Thus, leaner mixtures with lower temperatures and less EGR tend to improve the thermodynamic efficiency through a more advantageous  $\gamma$  value.

Concerning the HT, it is caused mainly by convection from the hot in-cylinder gases to the combustion chamber walls. HT is typically lower for LTGC engines than for conventional engines because of the lower combustion temperatures, a more quiescent flow field, reducing the convective HT-coefficient and the absence of radiation from soot<sup>5</sup>. However, HT still constitutes a significant part of the lost energy. Modeling works have shown that HT is sensitive to various main engine parameters [6, 15, 16]. In particular, HT was found to increase with CA50 being more advanced. Hence, this effect acts to mitigate the gain in  $\eta_{th}$  produced by the better expansion ratio, particularly as CA50 is closely approaching TDC, where the gain in expansion ratio is small. If CA50 is not sufficiently retarded to slow down the reaction rate, the combustion process can generate relatively strong acoustic oscillations (*i.e.* knock) [17]. If knocking conditions are encountered, the acoustic oscillations further enhance

the HT and can lead to significant decrease in the  $\eta_{th}$  [4, 18, 19]. The knock-limit often dictates the high-load boundary of the engine and also restrains the  $\eta_{th}$ . As pointed out by Saxena and Bedoya [6], a better quantitative understanding of how ringing/knock impacts the HT is required. More generally, for practical operations of LTGC engines, there is a lack of understanding regarding variations of HT with operating parameters and how these variations affect the  $\eta_{th}$ , in contrast to the  $\eta_{comb}$  and the thermodynamic efficiency which are fairly well understood.

This summary of the factors influencing the  $\eta_{th}$  in LTGC engines highlights the fact that the multiple tradeoffs can take place. In this context, the primary objective of the current study is to provide a detailed understanding of the trend in  $\eta_{th}$  with changes in key operating parameters by systematically analyzing variations in the main energy-loss terms. In this study, the parameters that have been selected are: CA50,  $\phi_m$ , intake temperature ( $T_{in}$ ) and engine speed. The effect of CA50 includes a characterization of the effect of knock on the HT (and  $\eta_{th}$ ) and an evaluation of two commonly employed knock-detection metrics (the knock index [20] and the ringing intensity [21]). Then,  $\phi_m$  is swept with CA50 adjusted to prevent knock. The analysis of the effects of these two fundamental parameters (CA50 and  $\phi_m$ ) will help to explain the influence of  $T_{in}$  and engine speed. Before presenting the results, the experimental setup is introduced in the next section. Following this, in the “Data Analysis” section, the methodology developed to compute the amount of energy lost through HT and into the exhaust is explained in detail.

## Experimental Setup & Data Acquisition

### Engine Facility

The LTGC research engine used for this study was derived from a Cummins B-series six-cylinder diesel engine with a displacement of 0.98 liters/cylinder. Figure 1a shows a schematic of the engine, which has been converted for single-cylinder operation. The engine specifications and main operating conditions are listed in Table 1. Data for the present study have been obtained using two different pistons, giving geometric CRs of 14:1 and 16:1, as shown in Figure 1b. Both pistons provide a small top ring-land crevice, amounting to less than 0.9% of the TDC volume.

As shown in Figure 1a, the EGR loop is equipped with a cooler, a gas-to-water heat exchanger and a gas/liquid separator (not shown) to remove the condensed water. The flow rate of cooling water can be adjusted to control the temperature of the EGR gases down to temperatures as low as 30°C. The EGR is introduced well upstream of the intake plenum, to insure that the intake charge is well mixed. With this configuration, the exhaust pressure must be greater than the intake pressure ( $P_{in}$ ) for EGR to flow into the intake. The required back pressure was achieved by throttling the exhaust flow using the valve shown in Figure 1a. This typically resulted in the exhaust pressure being about 2 kPa greater than  $P_{in}$ <sup>6</sup>. Intake air was supplied

<sup>4</sup> For boosted-LTGC engines, cooled-EGR is used as a control strategy to delay the CA50 in order to prevent knock with increased fueling [13], when it is not practical to further decrease  $T_{in}$ .

<sup>5</sup> In LTGC engines, the ability to phase most of the combustion sequence closely after TDC, due to the fast reaction rate, can also contribute to lower HT. As opposed to combustion igniting “well” before TDC, significant negative work is avoided, reducing the time for HT at higher in-cylinder temperatures.

<sup>6</sup> This exhaust pressure is much lower than would be required to drive an actual turbocharger. However, the current work focuses on changes in IMEP<sub>g</sub> which is hardly affected by using a higher, more-realistic exhaust pressure, as was shown in a previous study [13]. In this earlier work, a realistic back pressure, considering a 40% combined turbo and compressor efficiency for a  $P_{in} = 2.0$  bar condition, reduced the IMEP<sub>g</sub> by < 0.2% (or about a 0.1%-unit decrease in  $\eta_{th}$ ), which is in the noise of the data. Net IMEP was reduced by about 4%. Thus, not considering the higher exhaust pressure is not expected to significantly affect the ensuing results.

by an air compressor and precisely metered by a sonic nozzle as shown in Figure 1a. The EGR fraction was varied by adjusting the amount of supplied air, and then adjusting the exhaust throttle to maintain the desired  $P_{in}$ . In this article, all pressures are absolute.

Table 1. Engine specifications and operating conditions.

Displaced (single cylinder)	0.981 liters
Bore	102 mm
Stroke	120 mm
Connecting rod length	192 mm
Geometric compression ratio	14:1 & 16:1
Approximate surface to volume ratio at TDC [1/cm]	2.65 (CR = 14:1) 2.96 (CR = 16:1)
Number of valves	4
I/O	0°CA *
IVC	202°CA *
EVO	482°CA *
EVC	8°CA *
Swirl ratio	0.9
Fueling system	Fully PM and GDI
GDI injector	Bosch, 8-hole
Included angle	70°
Hole size	Stepped-hole, min. dia. = 0.125 mm
Injection pressure	120 bar
Engine speed	1000 to 2000 RPM
Centerline $T_{in}$ †	30 to 70°C
$P_{in}$ (abs.)	2.0 and 2.4 bar
Coolant and oil temperature	~ 100°C

\* 0°CA is taken to be TDC intake. The valve-event timings correspond to 0.1 mm lift.

†  $T_{in}$  is measured in the center part of the duct in the two runners about 120 mm from the intake valves.

In this study, both PreMixed (PM) and Direct Injection (DI) fueling were used. The PM fueling system, shown at the top of the schematic in Figure 1a consists of a GDI (Gasoline-DI) injector mounted in an electrically heated fuel-vaporizing chamber and appropriate plumbing to ensure thorough premixing with the air and EGR upstream of the intake plenum. The DI fueling is accomplished using a second GDI injector mounted centrally in the cylinder head. The amount of fuel supplied was measured with a volumetric fuel flow meter, calibrated in-house, taking into account liquid-compressibility effects and changes in density with temperature. The measurement error and repeatability of the fuel flow rate spans between +/- 0.2%. Depending upon the dataset presented in the results section, two different gasoline blends were used. Neither gasoline blend contained ethanol. The fuel specifications are listed in Table 2.

Prior to starting the experiments, the engine was preheated to 100°C by means of electrical heaters on the “cooling” fluid and lubricating-oil systems. In addition, the intake tank and plumbing were preheated to a minimum temperature of 60°C to avoid condensation of the fuel in the case of the PM fueling system. The minimum  $T_{in}$  in the case of the DI injection was 30°C. An auxiliary heater mounted close to the engine provided precise control of the  $T_{in}$ .

This work uses an equivalence ratio based on total charge mass, rather than air alone. This equivalence ratio, referred to as the charge-mass equivalence ratio ( $\phi_m$ ), is defined by Equation 2<sup>7</sup>, where  $F/C$  is the mass ratio of fuel and total charge gas (*i.e.* fresh air and EGR), and  $(F/A)_{stoich}$  is the mass ratio of stoichiometric fuel/air mixture for complete combustion. This provides a convenient and consistent way to compare data with the same supplied energy content per unit charge mass (*i.e.*, the same dilution level) for operating conditions with different fuels and different EGR levels. Note that  $\phi_m$  is the same as conventional air-based  $\phi$  when no EGR is used. It should also be noted that the air-based  $\phi$  is  $< 1$  for all conditions presented.

$$\phi_m = \frac{(F/C)}{(F/A)_{stoich}} \quad (2)$$

Prior to starting the experiments, the engine was preheated to 100°C by means of electrical heaters on the “cooling” fluid and lubricating-oil systems. In addition, the intake tank and plumbing were preheated to a minimum temperature of 60°C to avoid condensation of the fuel in the case of the PM fueling system. The minimum  $T_{in}$  in the case of the DI injection was 30°C. An auxiliary heater mounted close to the engine provided precise control of the  $T_{in}$ .

Table 2. Fuel properties.

	Chevron-Phillips Research-Grade Gasoline *	Haltermann Solutions Certification Gasoline
Antiknock Index (R+M)/2	86.9	92.7
RON	91.0	96.6
MON	82.7	88.7
Specific gravity	0.746	0.743
Carbon [wt%]	86.37	86.49
Hydrogen [wt%]	13.55	13.34
Oxygen [wt%]	0.08	None detected
A/F Stoichiometric	14.60	14.56
Lower Heating Value, gas-phase [MJ/kg]	43.10	42.97
LHV for stoichiometric charge [MJ/kg]	2.763	2.762
Hydrocarbon type [vol%]		
Aromatics	24.5	34.3
Olefins	5.1	0.12
Saturates	70.1	64.0
Distillation [°C]		
5%	56.9	43.3
10%	63.4	52.8
30%	78.9	80.6
50%	96.1	106.1
70%	114.1	117.8
90%	147.3	159.4
95%	164.9	172.8

\* Based on analysis provided by Paragon Labs, Inc.

<sup>7</sup> This definition is similar to the one used by other authors (*e.g.* [22]) denoted as  $\phi'$ , which additionally accounts for the residuals. For our engine, the residual gas fraction is small (lower than 4%-mass) so that  $\phi_m \approx \phi'$ .

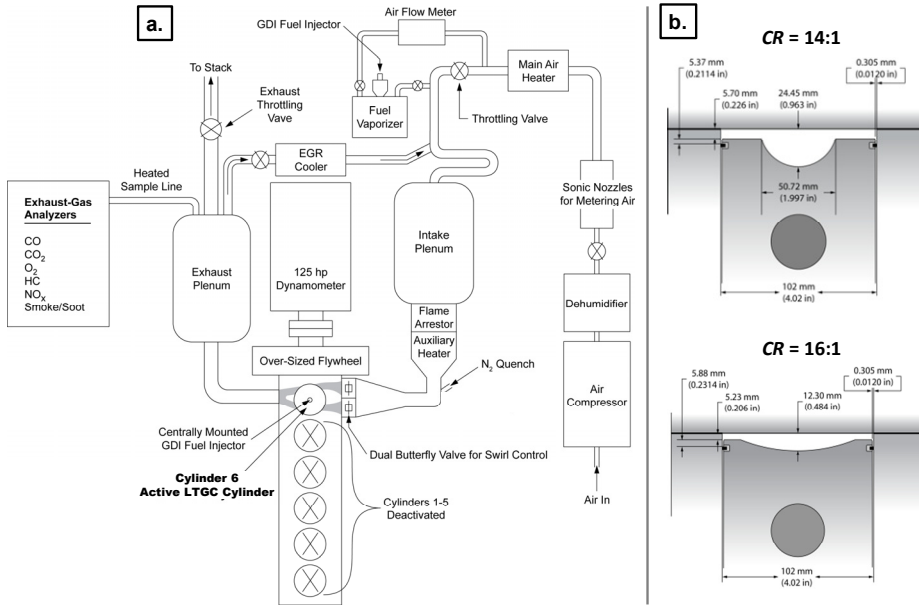


Figure 1. Schematic of the LTGC engine facility (a.) and combustion chamber geometries of the CR = 14:1 and 16:1 at TDC (b.).

## Data Acquisition

Cylinder pressure ( $P_{cyl}$ ) measurements were made with a transducer (AVL QC33C) mounted in the cylinder head approximately 42 mm off center. The pressure transducer signals were digitized and recorded at  $\frac{1}{4}^\circ$  CA increments for one hundred consecutive cycles. The cylinder-pressure transducer was pegged to the  $P_{in}$  near Bottom Dead Center (BDC) where the  $P_{cyl}$  reading was virtually constant for several degrees. Cycle-average firedeck temperatures were monitored with a  $K$ -type thermocouple embedded in the cylinder head so that its junction was about 44 mm off the cylinder center and 2.5 mm beneath the surface. Surface temperatures were estimated by extrapolating the thermocouple reading to the surface, using the thickness of the firedeck and assuming that the back surface was at the cooling-water temperature.  $T_{in}$  was monitored using thermocouples mounted in the two intake runners close to the cylinder head at the flow-centerline. Flow-centerline exhaust temperature was also measured with a thermocouple located about 200 mm from the exhaust valves. For all data presented,  $0^\circ$ CA is defined as TDC intake (so TDC compression is at  $360^\circ$ CA).

The CA of the 50% burn point (CA50) was used to monitor the combustion phasing. CA50 was determined from the cumulative Apparent Heat-Release Rate (AHRR), computed from the low-pass filtered cylinder-pressure data described below. Computations were performed for each individual cycle, disregarding HT and assuming a constant ratio of specific heats [23]. The average of 100 consecutive individual-cycle CA50 values were then used to monitor CA50 during engine operation and for the values reported. The low-pass filter was set so that frequencies below 2.5 kHz were unaffected, while frequencies from 2.5 to 3.9 kHz were progressively attenuated using a Gaussian roll-off function. This smoothly truncates the frequency power spectrum at the near-zero energy region between the lower frequencies due to combustion and the higher frequencies due to knock [8, 20].

The operating range of LTGC engines is often limited by the occurrence of knock, characterized by a distinctive sharp sound, an

increase in HT that reduces the  $\eta_{th}$  and could result in engine physical damage over time. In this work, the correlation for Ringing Intensity (RI, Equation 3) developed by Eng [21] is used to indicate the propensity for engine knock. The RI, expressed in  $MW/m^2$ , is a metric designed to correlate with the acoustic energy of the resonating pressure wave.

$$RI \approx \frac{1}{2\gamma} \cdot \frac{\left( \beta \cdot \left( \frac{dP}{dt} \right)_{max} \right)^2}{P_{max}} \cdot \sqrt{\gamma \cdot R \cdot T_{max}} \quad (3)$$

In this equation,  $(dP/dt)_{max}$ ,  $P_{max}$  and  $T_{max}$  are the peak values of the PRR (in real time: kPa/ms), cylinder pressure, and the mass-averaged charge temperature, respectively, and  $R$  is the gas constant. The Peak-PRR (PPRR)<sup>8</sup> was obtained from the individual low-pass-filtered pressure traces (with a linear fit over a moving  $\pm 0.5^\circ$ CA window), and converted to real-time using the average crankshaft speed, together with the peak mass-averaged temperature and pressure from the ensemble-averaged pressure trace. Based on our experience with this engine at all boost levels tested (*i.e.*  $P_{in} = 1.0$  to 3.2 bar [13]) and mainly at 1200 RPM, using  $\beta = 0.05$  ms as a constant (following Eng [21]), a RI criterion of  $5 MW/m^2$  was found to reasonably correlate over a range of conditions to the onset of an audible knocking sound and the appearance of obvious ripples on the pressure trace (maximum amplitude  $> \sim 1$  bar). For comparison, this RI threshold of  $5 MW/m^2$  selected for operation without knock corresponds to about  $8 \text{ bar}/^\circ\text{CA}$  at 1200 RPM (or  $58 \text{ bar/ms}$ ), naturally aspirated. With higher boost levels, higher PRRs can be used for the same audible knocking sound. This is taken into account in Equation 3 by the  $P_{max}$  term in the denominator. The use of a time-based PRR, as opposed to a CA-based one, is intended to eliminate the engine speed dependence on the onset of knock [21]. However,

<sup>8</sup> The time-based PRR is equivalent to  $(dP/dt)_{max}$  while the CA-based PRR is equivalent to  $(dP/d\theta)_{max}$ .

evidence provided in a recent study [20] and supported in the current study, suggest that the RI correlation might not be effective for large changes in engine speed.

Exhaust emissions data were also acquired, with the sample being drawn just downstream of the exhaust plenum using a heated sample line (See Figure 1a). CO, CO<sub>2</sub>, HC, NO<sub>x</sub>, and O<sub>2</sub> levels were measured using standard exhaust-gas analysis equipment. For all data reported (even for the knocking cases), NO<sub>x</sub> were well below (typically more than an order of magnitude) below the US-2010 limit (*i.e.* 0.27 g/(kW.h)). Soot emissions were monitored using an AVL smoke meter and found to be below the detectability limit for all data reported. A second CO<sub>2</sub> meter monitored the intake gases just prior to induction into the engine, which allowed the EGR fraction of the intake gases to be computed. The uncertainty in the exhaust gas measurement is reported to be less than ±1%.

## Data Analysis

Energy distribution analysis was performed on the “closed” part of the cycle from BDC-compression (180°CA) to BDC-expansion (540°CA). Considering the first law of thermodynamics, the supplied energy is split into the four following energy pathways<sup>9</sup>:

1. Gross-indicated thermal efficiency
2. Combustion inefficiency
3. Heat transfer
4. Exhaust losses (Exh-L)

HT and Exh-L have been evaluated with different methods presented below. This cross-checking was necessary in order to validate the observed trends.

## Gross Indicated Thermal Efficiency ( $\eta_{th}$ ) and Combustion Efficiency ( $\eta_{comb}$ )

The gross-indicated thermal efficiency, denoted as  $\eta_{th}$ , is the metric of primary interest in this study. The intention is to focus on the combustion-related phenomena and to avoid too much dependence on engine technology. In contrast to the brake thermal efficiency, the indicated thermal efficiency does not include the mechanical losses (friction, accessories driving forces, transmission losses, *etc.*). The term “gross” (as opposed to “net”) means that only the “closed” part of the cycle is considered. Thus, the efficiency does not include the pumping losses during the breathing part of the cycle (intake and exhaust strokes). All  $\eta_{th}$  reported in this article are based on the gross indicated work, as determined from the IMEP<sub>g</sub> (gross-Indicated Mean Effective Pressure) and are defined as:

$$\eta_{th} = 100 \times \frac{\text{Gross indicated work}}{LHV_f \times m_f} \quad (4)$$

where LHV<sub>f</sub> is the Lower Heating Value of the fuel supplied, and m<sub>f</sub> is the mass of fuel.

$\eta_{comb}$  is defined as:

$$\eta_{comb} = 100 - 100 \times \frac{m_{HC} \times LHV_f + m_{CO} \times LHV_{CO}}{LHV_f \times m_f} \quad (5)$$

where m<sub>HC</sub> and m<sub>CO</sub> are the mass of the corresponding pollutant species determined from emission measurements.

## Heat Transfer (HT)

Three methods have been evaluated to estimate the HT:

### Method 1 (Instantaneous):

The total-HT is estimated by considering the general expression for instantaneous, spatially averaged HT (Equation 6). This equation is particularly representative of the global as well as local HT behavior in HCCI-like engines because of the high degree of homogeneity in the HT throughout the combustion chamber for such engines, as demonstrated by Chang et al. [24].

$$Q_w[J] = \frac{60/360}{RPM} \times \int_{180}^{EVO=482} h(\theta) \times A(\theta) \times (T_{gas}(\theta) - \bar{T}_w) \cdot d\theta \quad (6)$$

In equation 6, Q<sub>w</sub> is the total-HT (here in [J]), h is the HT-coefficient deduced from a global model detailed below, A is the exchange surface area, and T<sub>gas</sub> is the mass-average charge temperature which varies over the cycle and is obtained from the ideal gas law considering real gas properties (*i.e.* variable  $\gamma$ ) and  $\bar{T}_w$  is the cycle averaged wall surface temperature which was taken to be the extrapolated firedeck temperature as introduced in the “Data Acquisition” section. Regarding HT-coefficient, several empirical / semi-empirical correlations have been proposed and modified to estimate this quantity [18, 23-30]. Among them, the original Woschni correlation [23, 25, 28] has been used in this study because it is still relevant for determining HCCI-like HT as it is shown in the following.

The Woschni correlation is derived from the dimensionless expression of the form Nu = C × Re<sup>m</sup> (Nu and Re being respectively the Nusselt and Reynolds numbers, C and m the scaling constants) for forced steady turbulent convection HT. The Woschni correlation is expressed as (Equation 7):

$$h_{Woschni}(\theta) \left[ \frac{W}{K \cdot m^2} \right] = C_m \times B^{-0.2} \times P_{cyl}(\theta)^{0.8} \times T_{cyl}(\theta)^{-0.53} \times [C_1 \times \bar{P}_s + C_2 \times (P_{cyl}(\theta) - P_{cyl} \text{ "motor " }(\theta))]^{0.8} \quad (7)$$

where C<sub>m</sub> is the main coefficient, the diameter of the bore B is the characteristic length scale, T<sub>cyl</sub> is the mass-average gas temperature. T<sub>cyl</sub> and P<sub>cyl</sub> take into account the change in the physical properties of the charge-gas (density, viscosity and heat conductivity) with temperature and pressure. In addition, the temperature term includes the influence of radiation on the HT in a lumped form with the convective effect [25]. However, the radiation effect is likely to be small because of the soot-free and low combustion temperatures in typical LTGC engines.

<sup>9</sup> See Footnote #3 regarding the blow-by.

The term in the square bracket to the power 0.8 ( $0.8 = m$  in the Nusselt expression stated above) represents the mean gas velocity.

The first part of this term ( $C_1 \times \overline{P}_S$ ) represents the gas velocity for a motored engine (unfired) with  $C_1$  described by Equation 8 which takes into account the mean piston speed  $\overline{P}_S$  and the swirl ratio  $S$ .

$$C_1 = 2.28 + 0.308 \times \frac{\pi \cdot B \cdot \text{RPM}/60 \cdot S}{\overline{P}_S} \quad (8)$$

The second part of the velocity term in Equation 7 represents the combustion-induced gas velocity scaled with  $C_2$ . It is proportional to the difference between the  $P_{cyl}$  trace under fired and motored conditions. For every operating condition (every set of  $T_{in}$ ,  $P_{in}$ , RPM), 100 consecutive motored pressure traces are acquired, pegged, filtered and averaged, with only supplying dry air to the engine. However, this motored  $P_{cyl}$  is not directly used in Equation 7, otherwise this would result in an artifact during the compression stroke. Indeed, the combustion-induced term in Equation 7 would return a non-zero value during compression because the pressure signals of the fired and motored cycles do not overlap as seen in Figure 2. This is because  $\gamma$  of the charge is always lower for the fired case (presence of fuel, residuals and eventually EGR, with higher gas temperature). Therefore, as shown in Figure 2, the “motored  $P_{cyl}$ ” used in Equation 7 first tracks the  $P_{cyl}$  of fired case during the compression stroke up to the point where both traces intersect. Then, Equation 7 uses the actual measured motoring  $P_{cyl}$ .

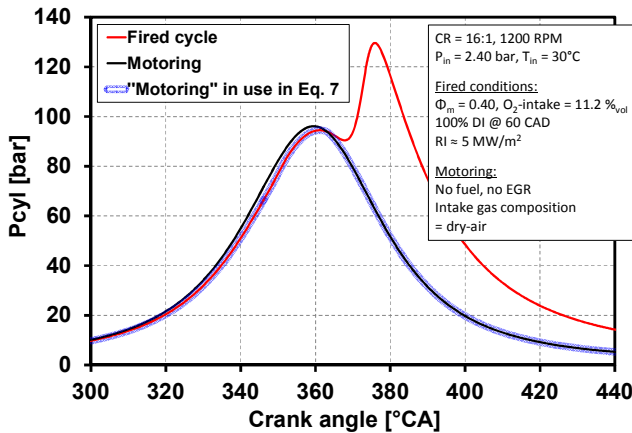


Figure 2: Comparison of the  $P_{cyl}$  traces in motoring and fired conditions and illustration of the “motoring”  $P_{cyl}$  used in the HT correlation.

The values for the coefficients  $C_m$  and  $C_2$  in Equation 7 must still be determined. The main scaling coefficient,  $C_m$ , is engine specific [24, 25]. In contrast,  $C_2$ , the scaling coefficient for the combustion-induced velocity term, is sensitive to the intensity of the turbulence generated by the combustion event [25] and is believed to be somewhat dependent to the combustion mode (flame propagation, diffusive flame, sequential autoignition, mixed-modes) and the presence of combustion-induced acoustic oscillations [18].

It has often been reported that using the Woschni correlation with the original values for  $C_m$  and  $C_2$  (adjusted for a Diesel engine in 1967 [25]) is inappropriate to assess the HT for HCCI-like LTGC engines [24, 29-31]. Chang *et al.* [24] conducted measurements of HT in an HCCI engine and modified the Woschni correlation accordingly. They found that  $C_2$  needs to be significantly reduced (*i.e.* divided by 6) for HCCI-like combustion compared to the Woschni original

value. They also use the instantaneous chamber height as the characteristic length scale (the bore in original Woschni) and the temperature exponent is recalibrated to be -0.73. A comparison between the original Woschni and this modified version by Chang *et al.* will be provided in a following subsection.

The values of the coefficients  $C_m$  and  $C_2$  are adjusted to our engine platform and operating conditions using a two steps approach explained in the following. In a first step,  $C_m$  is adjusted by matching the output of Equation 6 to the total-HT determined experimentally by computing the AHRR on a motored cycle (Figure 3). In this manner,  $C_2$  is not participating since the combustion-induced velocity term is equal to zero.

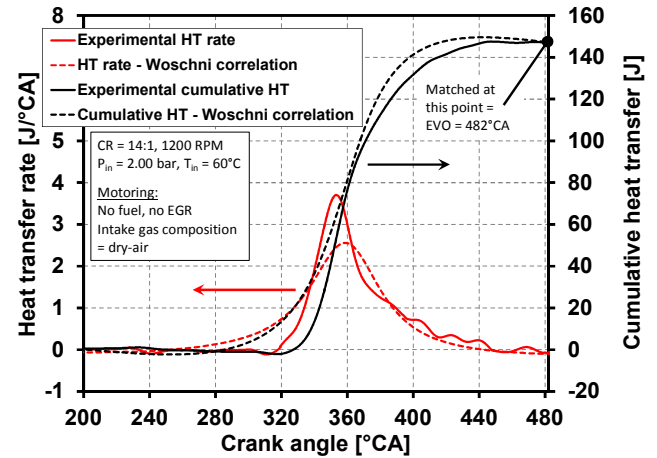


Figure 3: Comparison under motored condition of the HT-rate and cumulative-HT between the experiment and the computation after adjusting  $C_m$  in the HT correlation to match the experimental total-HT.

In a second step, with  $C_m$  fixed at the value computed from the motored  $P_{cyl}$ , the value of  $C_2$  is determined from the fired cycle data. This is accomplished by adjusting  $C_2$  until the cumulative-HR corrected for HT matches the burned energy as described by Equation 9. This adjustment is illustrated in Figure 4. In our methodology, at the start of the combustion (first point shown in Figure 4), the cumulative corrected-HRR is set to zero and the integration is performed until the end of combustion (second point in Figure 4). Note that the exact values for the limits of integration are not critical since the corrected-HRR is nearly flat beyond these points (Figure 4a).

$$m_f \times LHV_f \times \eta_{comb} = (cum. gross. HR)_{end of comb} = (cum. AHR + cum. HT)_{end of comb} \quad (9)$$

It was found that the optimization of the value of  $C_2$  needs to be repeated for every experimental point so that the energy balance described by the Equation 9 is always satisfied. Similarly,  $C_m$  needs to be readjusted only when one of the main operating conditions (*e.g.*  $T_{in}$ ,  $P_{in}$ , RPM) is modified. The value of coefficients  $C_m$  and  $C_2$  was found to significantly vary as operating conditions were changed. This will be shown in the results section for  $C_2$  in Figure 7. Modifying the original correlation and accurately calibrating the coefficients and exponents to make it predictive over the wide range of operating conditions covered in this work is out of the scope of this study. One major concern is the need to include in the combustion-induced velocity term, a parameter to model the effect of

the intensity of the acoustic oscillations, as done by Tsurushima *et al.* [18]. In this current work, the information that is not captured by the terms in the correlation like knock is included by a variation of the value of the coefficients. Carefully adjusting the coefficients for every operating point provides a mean to determine fairly well the HT. Indeed, the energy balance equation is always satisfied and as the example in Figure 4a shows, the HRR is well-corrected (the corrected-HRR is nearly flat before and after the combustion event). Moreover, as it will be discussed in conjunction with Figure 6, the total-HT derived from the Woschni correlation was found to be in good agreement with that determined by two others methods introduced below. Finally, trends in the variation of the HT-coefficients provide additional information as will be discussed.

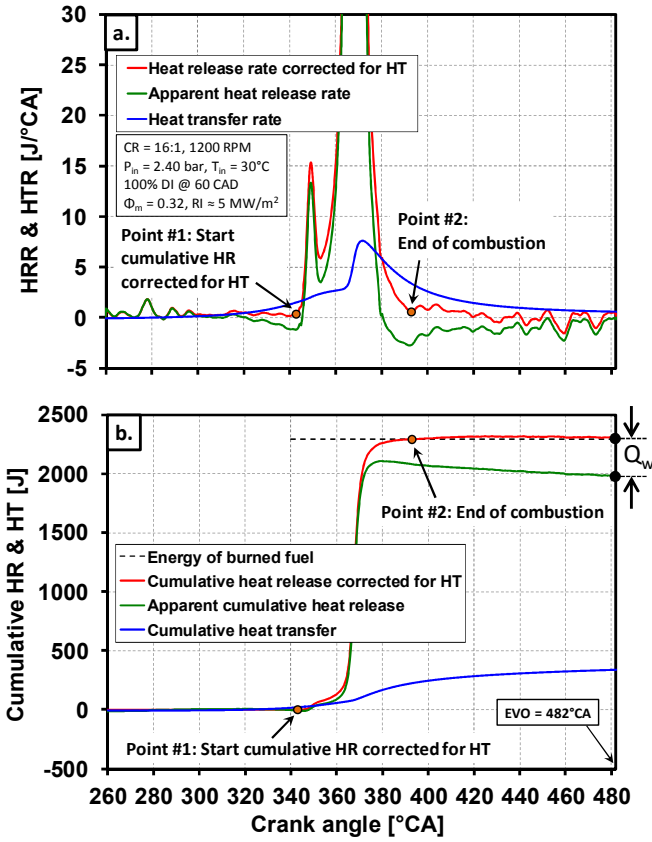


Figure 4: Heat release rate (a.) and cumulative heat release (b.) profiles (apparent and corrected for HT).

### Method 2 (Global average):

As evident from Figure 4b, the total-HT can also be simply estimated by the difference between the total energy of the burned fuel and the cumulative of the AHRR (Equation 10) until EVO (*i.e.* 482°CA).

$$Q_W = m_f \times LHV_f \times \eta_{comb} - cum. AHRR_{@EVO} \quad (10)$$

Note that for methods 1 and 2, the computation cannot be performed for CA later than EVO because it is the latest CA for which the ideal gas law still holds (assuming a constant charge-mass during the cycle). This implies that the HT from EVO to BDC is not considered. Thus, the HT is likely to be under-valued for these methods, but, estimates indicate that HT from EVO to BDC represents no more than 1% of the total fuel energy.

### Method 3 (Global average):

The fraction of HT (HT in [% of total supplied energy]) can be estimated as the remainder of the first law energy balance equation (Equation 11), knowing the fraction of heat lost into the exhaust Exh-L (detailed in the next subsection).

$$\eta_{th} + (100 - \eta_{comb}) + HT + ExhL = 100 \quad (11)$$

### Exhaust Losses (Exh-L)

Three methods have also been evaluated to estimate the amount of energy lost into the exhaust.

#### Method 1:

The energy balance equation 11 is applied to indirectly calculate the Exh-L, using the HT-losses obtained with equation 6 (Method 1 or 2 for HT).

#### Method 2:

The measured exhaust temperature  $T_{exh}$  is used to compute the sensible enthalpy of exhaust gas  $\Delta h_{exh}$  in [J]. The enthalpy change between the enthalpy in the exhaust gas (final enthalpy) and a reference-state enthalpy (initial enthalpy) taken at BDC-intake (*i.e.* 180°CA) is calculated. This is illustrated in Figure 5 (between points 1 & 2) and defined by equation 12,

$$\Delta h_{exh} = m_c \times (c_p(exh. gas @ T_{exh}) \times T_{exh} - c_p(int. gas @ T_{BDC}) \times T_{BDC}) \quad (12)$$

where  $m_c$  is the charge-mass per cycle and  $c_p$  is the specific heat capacity at constant pressure which depends on the gas composition and the temperature.  $T_{BDC}$  has been estimated using the procedure developed by Sjöberg and Dec [32] accounting for HT during induction.

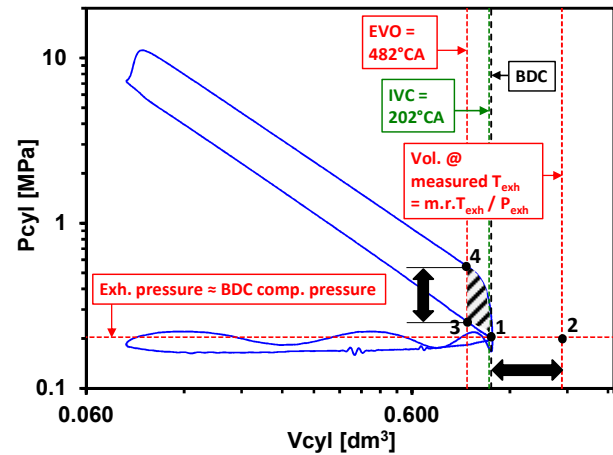


Figure 5: Log-log PV cycle representing the computation of the Exh-L 1) through the measured exhaust temperature (between points 1 & 2: method 2) and 2) through the computed EVO temperature (between points 3 & 4: method 3).

One drawback of this method is that the measured- $T_{exh}$  is sensitive to the location of the temperature sensor in the exhaust runner.  $T_{exh}$  is affected by the amount of HT during the exhaust stroke<sup>10</sup> and in the exhaust system before reaching the thermocouple. Therefore, the Exh-L would tend to be underestimated.

### Method 3:

A third method to compute the Exh-L is introduced to tackle the drawback of using the measured  $T_{exh}$ . Instead of using the measured  $T_{exh}$ , the mass-averaged charge temperature at EVO obtained using cycle analysis is used. The computation is also performed at EVO because it is the last CA for which the ideal gas law still holds. The internal energy change  $\Delta u_{exh}$  in [J] is then computed (Equation 13) between the conditions at the CA of EVO and the corresponding CA in the compression stroke at iso-volume (as seen in Figure 5 between points 3 at 238°CA & 4).

$$\Delta u_{exh} = m_c \times (c_{v(exh. gas @ T-EVO)} \times T_{EVO} - c_{v(int. gas @ T-238)} \times T_{238}) - W_{(EVO \rightarrow BDC \& BDC \rightarrow 238)} \quad (13)$$

where  $c_v$  is the specific heat capacity at constant volume which depends on the gas composition and temperature. From this internal energy change, it is necessary to subtract the amount of work represented by the cross-hatched area in Figure 5 between BDC to the points 3 and 4, otherwise the Exh-L would be significantly overestimated. However, HT between points 3 - 4 to BDC is still not accounted. Thus, the Exh-L is slightly overestimated.

### Comparison of the Different Methods

Figure 6 compares the output of the different methods in terms of HT for an example of a  $\phi_m$  sweep that will be fully described in the “Results” section. Indirect methods using the Exh-L and the energy balance equation 6 are shown with dashed-lines/open-symbols while the methods directly estimating the HT are shown with continuous-lines/ filled symbols. Reasonable agreement is obtained between these different methods. The trends are similar, particularly among the methods that directly compute the HT (curves nearly parallel). Between all methods, the magnitude of the HT is within 6-7% at most, and less than 3% without considering the method using the  $T_{exh}$ . The HT-trend determined using  $T_{EVO}$  has a slightly higher slope. As mentioned earlier, the method using  $T_{exh}$  underestimates the Exh-L. As a result, HT tends to be overestimated. Also, generally the trends appear noisier and the slope is also significantly different from the other methods as seen in Figure 6.

The HT determined from the other methods is likely to be underestimated because they do not consider the HT from EVO to BDC. As mentioned earlier, this omission is responsible of an error less than 1%. A comparison was performed between the Woschni correlation and its modified version by Chang *et al.*, introduced earlier. As for the Woschni correlation, we found that the coefficients  $C_m$  and  $C_2$  were also needed to be significantly varied in order to satisfy the energy balance equation. Overall, as seen in Figure 6, even

though some datapoints were skipped, the trends given by these two correlations are nearly identical. The difference was found to be attributed to the way these models distribute the HT-rate.

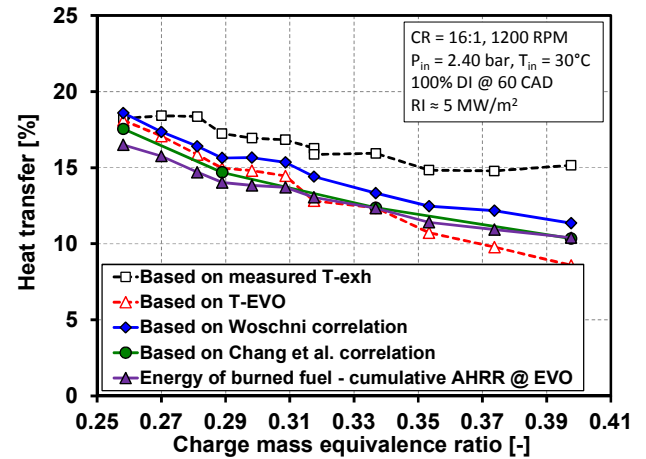


Figure 6: Comparison of the different methods to estimate the total-HT. Example of a  $\phi_m$  sweep at  $RI = 5 \text{ MW/m}^2$ .

Without direct measurements of the heat flux, which is out of the scope of this study, it is not easy to determine the most accurate method. However, the method using the Woschni correlation is thought to provide the best estimate since it provides values lower than the method using  $T_{exh}$  (known to be overestimated) and gives the highest values among the methods that are likely to underestimate the HT. Moreover, multiple repetitions of engine tests at given operation conditions show that the results are more repeatable for the methods directly computing the HT compared to the method using  $T_{EVO}$ . This is probably due to slight day-to-day discrepancies in measuring the flow rates of gases supplied to the engine which affects the calculation of the enthalpy and the internal energy (Methods 2 & 3 for Exh-L). As shown in the Appendix 1, the repeatability in computing the HT using the Woschni correlation is +/- 0.5%.

Thus, in the following, the HT computed from the Woschni correlation is designated as the reference. The other methods were used in order to always validate the trend in HT with varying operating parameters. Finally, the use of the HT-coefficient correlation is advantageous because it enables more insight into the HT phenomenon through a visualization of the CA-resolved variations in the HT-rate and HT-coefficient.

## Results & Discussion

### Influence of CA50 and Knock at Fixed $\phi_m$ on the Energy Distribution

#### Introduction of the Operating Conditions and Characterization of Knock Onset Point

To investigate the effect of CA50 on the  $\eta_{th}$ , two sweeps were conducted at different  $\phi_m$  ( $= 0.32$  &  $0.42$ ).  $T_{in}$  was held constant at 60°C and CA50 was swept by varying the EGR rate. Reducing the EGR increases the overall reactivity of the mixture and thus leads to more advanced CA50. Experimental conditions for these two sweeps are summarized in Table 3. With CA50 being more advanced at constant  $\phi_m$ , the PPRR increases, as does the RI and thus the

<sup>10</sup> Considering the breathing part of the cycle is not desirable in this study because the energy distribution analysis is carried out on the “closed” part of the cycle.

propensity to knock (see Equation 3). The knock threshold for our platform is  $\sim 5 \text{ MW/m}^2$  as explained in the ‘‘Data Acquisition’’ section. In Figure 7, the RI is plotted along with a second commonly used knock metric, the KI (Knock Index). The KI is essentially a measure of the energy of the ripples on the  $P_{\text{cyl}}$ . It is obtained by integrating the amplitude of power spectral density (*i.e.* Fourier transform of the  $P_{\text{cyl}}$ ) of the first resonant mode [20]. The values of  $C_2$  (Equation 7), which scales the combustion-induced velocity term in the Woschni correlation, were optimized as explained in the ‘‘Data Analysis’’ section and are also shown in Figure 7. Note that a metric characterizing the overall combustion noise such as the CNL, also commonly used in the literature to limit the operating range for excessive noise, was intentionally not considered in Figure 7, since it has been proven to not be sensitive to the knock-induced noise [20].

Table 3: Operating conditions for the CA50 effect (at constant  $\phi_m$ ) on the  $\eta_{\text{th}}$ .

Geometric CR [-]	14:1	
Engine speed [RPM]	1200	
$P_{\text{in}}$ [bar] (+/- 0.01 bar)	2.0	
$T_{\text{in}}$ [°C] (+/- 1°C)	60	
$\phi_m$ [-]	0.32	0.42
$\text{O}_2$ -intake [% $_{\text{vol}}$ ]	18.0 $\rightarrow$ 19.2	14.4 $\rightarrow$ 14.7
Mean IMEP $_g$ [bar] (varies with $\eta_{\text{th}}$ )	$\sim 8.6$	$\sim 10.8$
Fuel	Research-Grade Gasoline	
Fueling strategy	Premixed	

For  $\phi_m = 0.32$ , the substantial increase in the KI coincides well with the  $\text{RI} \approx 5 \text{ MW/m}^2$  criterion for knock. However, for  $\phi_m = 0.42$ , the KI trend does not feature a distinctive change of slope at  $\text{RI} \approx 5 \text{ MW/m}^2$ . However, from a user standpoint of view, the sharp sound characteristic of knock starts to be emitted just above  $\text{RI} \approx 5 \text{ MW/m}^2$ . Then, the engine is clearly heavily knocking as RI ramps up to  $14 \text{ MW/m}^2$ . The reason that KI does not respond to this knock onset is thought to be related to the orientation of the first-mode wave, which is highly directional to the pressure transducer [33, 34]. This behavior is likely to occur in our engine as supported by the evidences provided in ref. [20]. In the following, a comparison with the trend of  $C_2$  supports that knock occurs for  $\text{RI} > 5 \text{ MW/m}^2$  for both  $\phi_m$ .

As seen in Figure 7, the value of  $C_2$  increases significantly above  $\text{RI} \approx 5 \text{ MW/m}^2$ . This means that the contribution of the combustion-induced turbulence term to the HT-coefficient has greatly increased. As it will be shown in conjunction with Figure 8b and Figure 9, this correlates with a substantial increase in the HT. In particular, knock has been shown to enhance the HT and to lower the  $\eta_{\text{th}}$  [4, 18, 20]. Winkler [19] found that the mechanism for the enhanced HT is the rapid transport of high-temperature fluid from the heat source towards the wall by the velocity fluctuations produced by the resonating pressures waves, with a possible effect on a smaller scale of the break-down of the boundary layer. This produces a rapid increase in the HT-coefficient, as interpreted by Grandin and Denbratt [35], and particularly the combustion-induced velocity term in the HT correlation (Figure 9c). Hence, this analysis supports that for RI beyond  $5 \text{ MW/m}^2$ , the magnitude of the acoustic oscillations is sufficiently strong to not only produce unacceptable noise but also to substantially increase the HT. For our engine, at these conditions, RI

$\approx 5 \text{ MW/m}^2$  is therefore a well-suited criterion as the limit for acceptable acoustic oscillations.

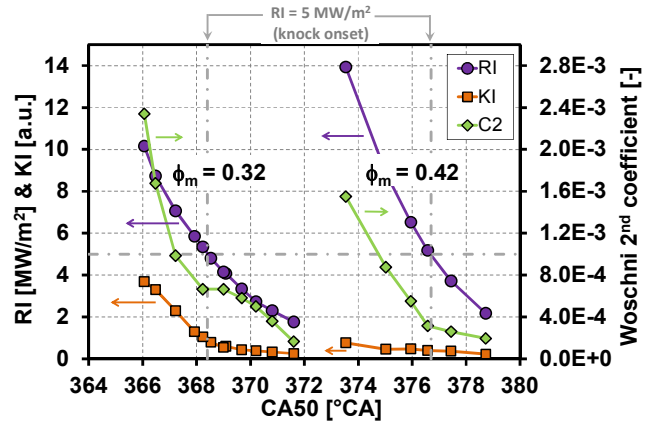


Figure 7: RI, KI and values of the 2<sup>nd</sup> Woschni coefficient (in the combustion-induced velocity term) as a function of CA50 (varied with EGR) at two  $\phi_m$ . See Table 3 for operating conditions.

Finally, these results show that analysis of the trends in the HT-coefficient consistently provide a better indicator of the onset of knock than the KI. Indeed, rather than being limited by the directional orientation of the pressure wave as with the KI, the HT and the HT-coefficient provide spatially-integrated measurements of the knock effect.

### Energy Distribution and Details on the HT

Figure 8 shows the effect of CA50 on the energy distribution ( $\eta_{\text{th}}$ ,  $\eta_{\text{comb}}$ , HT and Exh-L) for the two  $\phi_m$ . For  $\phi_m = 0.32$ , with CA50 being more advanced,  $\eta_{\text{th}}$  increases through a maximum and then decreases. This reversal in the  $\eta_{\text{th}}$ -trend coincides with the onset of knock. For  $\phi_m = 0.42$ , the range of CA50 spanned is more retarded. CA50 was not further advanced beyond  $\text{RI} \approx 14 \text{ MW/m}^2$  to prevent engine damage. For this sweep,  $\eta_{\text{th}}$  increases with more advanced CA50, but at a decreasing rate once knock occurs. For this higher  $\phi_m$ , the maximum  $\eta_{\text{th}}$  has not yet been reached for the most advanced CA50 because CA50 spans in a more retarded range, thus benefiting of a larger change in expansion ratio. In contrast, for  $\phi_m = 0.32$ , because the CA50 is so advanced that the gain in expansion ratio is smaller.

With advancement of CA50, the higher in-cylinder temperatures lead to a better  $\eta_{\text{comb}}$  (Figure 8a). The effect that this increase in  $\eta_{\text{comb}}$  alone would have on the  $\eta_{\text{th}}$  is also plotted, as computed with Equation 14. This equation is based on the principle that a change in the  $\eta_{\text{comb}}$  would affect the  $\eta_{\text{th}}$  proportionally to the fuel conversion efficiency (*i.e.* the  $\eta_{\text{th}}$ ). For instance, a change by 1%-unit of the  $\eta_{\text{comb}}$  would increase the  $\eta_{\text{th}}$  by 0.5%-unit if the  $\eta_{\text{th}}$  is 50%. Note that Equation 14 shows the improvement in  $\eta_{\text{th}}$  relative to the most retarded point (‘‘reference point’’) on each curve, the variable  $x$  in Equation 14 being CA50 for this dataset:

$$\text{Estimated } \eta_{\text{th}}(x) = \eta_{\text{th}, \text{ref.pt.}} \times \left( 1 + \frac{\eta_{\text{comb}}(x) - \eta_{\text{comb}, \text{ref.pt.}}}{100} \right) \quad (14)$$

Higher  $\eta_{\text{comb}}$  tends to increase the  $\eta_{\text{th}}$ . However, the trend is relatively weak and does not explain the main features of the  $\eta_{\text{th}}$  curve.

As seen in Figure 8b, advancing CA50 causes the HT to increase with a substantially faster rate once knock occurs. The HT increases by  $\sim 0.3$  to  $0.5\%$ -units per  $^{\circ}\text{CA}$  for non-knocking conditions and by  $\sim 0.8$  to  $1.2\%$ -units per  $^{\circ}\text{CA}$  once knock occurs. This acts to lower the  $\eta_{\text{th}}$ . The drop of the  $\eta_{\text{th}}$  at  $\phi_m = 0.32$  and the reduced rate of increase in  $\eta_{\text{th}}$  at  $\phi_m = 0.42$  correlate with the rapid increase in the HT once knock occurs. As represented by  $C_2$  in Figure 7, the main effect that causes the fast enhancement of the HT once knock occurs is the fast increase in the HT-coefficient during combustion. This is further supported by the data in Figure 9 showing that the charge temperatures hardly change, so the higher HT is caused by the increased HT-coefficient, and the overall HT-coefficient plotted in Figure 9 (Equation 7) tracks variations in  $C_2$ , the scaling coefficient for the combustion-induced velocity. Note that the change in the peak HT-coefficient per unit change in CA50 (*i.e.*  $\Delta\text{HT-coefficient}/\Delta\text{CA50}$ ) during combustion, deduced from Figure 9, increases by more than 370% from non-knocking to knocking conditions. In the non-knocking regime, the increase in the HT with more advanced CA50 is likely to be caused by a combination of a progressive increase in the peak  $\Delta T$  ( $T_{\text{gas}} - T_{\text{wall}}$ ) as well as by a slight increase in the HT-coefficient (Figure 9). Whereas, in the knocking regime, the HT increase is dominated by the greater increase in the HT-coefficient.

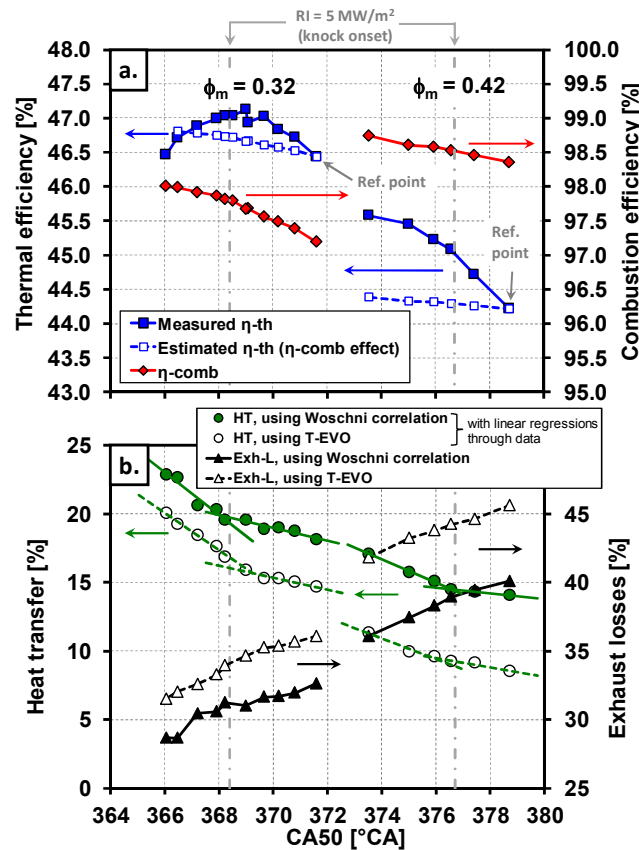


Figure 8: Effect of CA50 on the energy distribution at constant  $\phi_m$ . (a.):  $\eta_{\text{th}}$  and  $\eta_{\text{comb}}$ . Estimated- $\eta_{\text{th}}$  shows the trend in  $\eta_{\text{th}}$  from the reference point indicated in the plot by only considering the change in  $\eta_{\text{comb}}$  (b.): HT and Exh-L estimated with two different methods. See Table 3 for operating conditions.

Meanwhile, the Exh-L (Figure 8b) decreases almost linearly with CA50 advancement. A detailed discussion of this trend and its impact on the  $\eta_{\text{th}}$  are provided in the next subsection.

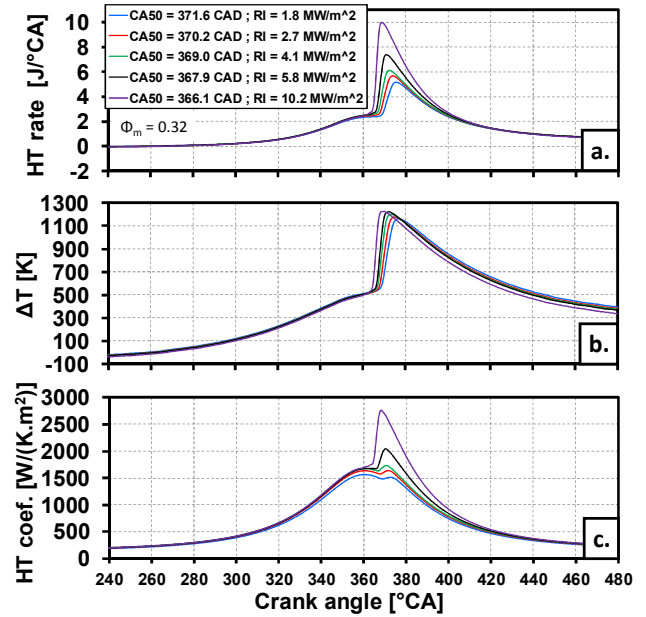


Figure 9: CA50 effect at  $\phi_m = 0.32$  on the HT rate (a.), the  $\Delta T$  (b.) and the HT coefficient (c.) evaluated using the Woschni correlation. See Table 3 for operating conditions.

### Insight into the Exh-L

It is of interest to understand the factors contributing to the Exh-L and how their magnitudes vary over the CA50 sweeps. Four main factors affecting the Exh-L are considered. They are the effects due to variations in 1)  $\eta_{\text{comb}}$ , 2) HT, 3) expansion ratio and 4)  $\gamma$ . These are plotted in Figure 10. The magnitude of their effect on the Exh-L was determined as detailed in the following. For the contributions from changes in  $\eta_{\text{comb}}$  and HT, their impact on the Exh-L is based on redistributing the changes in the fraction of fuel energy associated with these factors relative to a reference condition, into the other energy pathways, for instance:

- Variations in  $\eta_{\text{comb}}$  affect the  $\eta_{\text{th}}$ , the HT and the Exh-L. As mentioned above, for example, an increase in  $\eta_{\text{comb}}$  by + 1%-unit will contribute to an increase the  $\eta_{\text{th}}$  of  $\sim 0.5\%$ -unit if  $\eta_{\text{th}} \approx 50\%$ . Then, the remainder of the increase in  $\eta_{\text{comb}}$  will be split into the HT (+  $\sim 0.2\%$ -unit if HT  $\approx 20\%$ ) and into the Exh-L (+  $\sim 0.3\%$ -unit if Exh-L  $\approx 30\%$ ).
- In a similar manner, a decrease in HT acts to increase the  $\eta_{\text{th}}$ . However, the remainder of the decrease in HT will be only lost into the exhaust. If  $\eta_{\text{th}} \approx 50\%$  and Exh-L  $\approx 30\%$ , about 60%<sup>11</sup> of the decrease in HT is expected to increase the  $\eta_{\text{th}}$ , and the left-over goes into the Exh-L.

<sup>11</sup>  $60\% = 50/(50+30) \times 100$   
50% being the  $\eta_{\text{th}}$  and 30% the Exh-L.

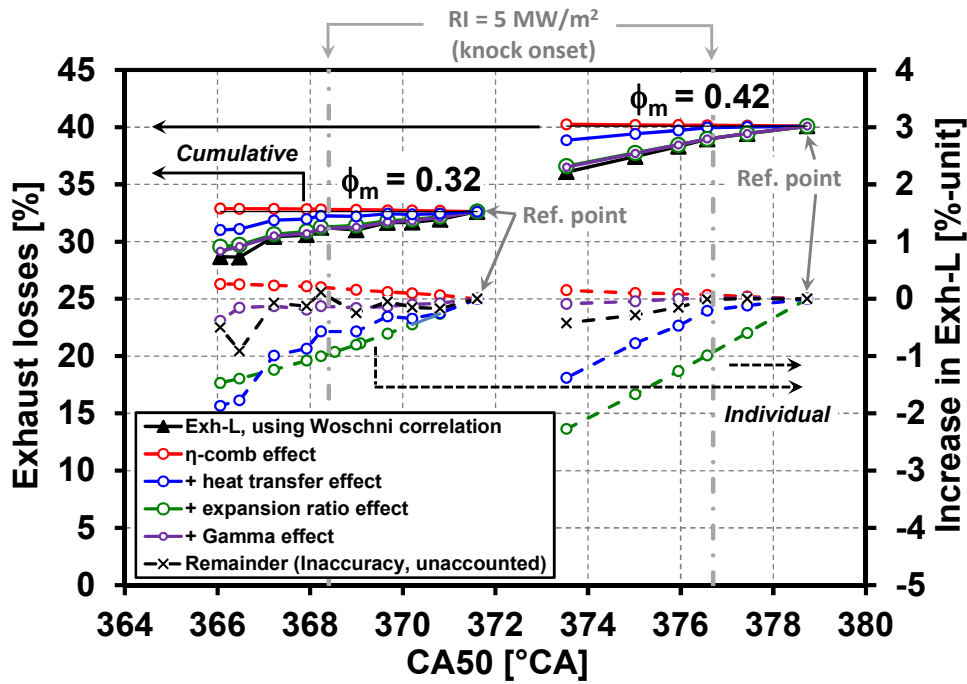


Figure 10: Detailed effect of CA50 on the Exh-L at constant  $\phi_m$ . Individual and cumulated contributions of  $\eta_{\text{comb}}$ , HT, expansion ratio and  $\gamma$  are shown from a reference point. See Table 3 for operating conditions.

For the data in Figure 10, the variations in the Exh-L due to individual changes in  $\eta_{\text{comb}}$  or HT have been determined using the actual fractions of the different energy pathways ( $\eta_{\text{th}}$ ,  $\eta_{\text{comb}}$ , HT, Exh-L). For more accurate calculations, the mathematical expressions provided in Appendix 2 are used. In these equations, variations are applied incrementally from the reference point noted in Figure 10. The other two factors that affect the Exh-L are, first, the combustion phasing, as indicated by the CA50 and second,  $\gamma$ . As explained in the introduction, both directly affect the amount of energy that can be extracted as work during the expansion process. For instance, a more retarded CA50 would decrease the effective expansion ratio and thus would decrease the work extracted, and hence, the  $\eta_{\text{th}}$ . This energy will directly be lost into the exhaust. Similarly, a lower  $\gamma$  would also decrease the amount of work extracted during expansion (and thus  $\eta_{\text{th}}$ ) and increase the Exh-L. The magnitudes of these effects have been assessed using Equation 1.

Figure 10 shows the effect of these four factors on the total Exh-L. For each  $\phi_m$  (0.32 and 0.42), there are two plots. The bottom plot (dashed lines) shows the individual contribution of each factor to the Exh-L relative to the reference point. The top plot (thin continuous lines) shows the cumulative effect obtained by adding each individual effect in the same order as given in the legend. In this case, the effect of  $\gamma$  is added last. The continuous black curve with triangle symbols is the amount of Exh-L reproduced from Figure 8b. When these four effects are added-up, an acceptable closure of the independently determined Exh-L is obtained. The remainder which is the difference between the Exh-L from the Woschni analysis and the Exh-L when all contributions described above are added-up is  $< 1\%$ -unit. This gives us confidence that we have accounted for all the factors affecting the Exh-L trend with reasonable accuracy.

As expected, as CA50 is advanced, the increase in the  $\eta_{\text{comb}}$  tends to increase the Exh-L (red curve). However, the decreasing trend in Exh-L is explained by a combination of the increasing fraction of HT (so a lower fraction of energy is lost into the exhaust) as shown by the blue curve, and also due to the better expansion ratio (green curve). Finally, the effect of  $\gamma$  is almost negligible (purple curve). This is because the higher mass-averaged temperature (which tends to reduce  $\gamma$ ) is compensated by the lower EGR (which acts to improve  $\gamma$ ) required to achieve this CA50 sweep. Finally, by comparing the individual effect of the expansion ratio for the  $\phi_m = 0.32$  and 0.42 datasets, it can be seen that, this effect is more pronounced at  $\phi_m = 0.42$  (2.3%-unit decrease in Exh-L) than at  $\phi_m = 0.32$  ( $\approx 1.5\%$ -unit decrease in Exh-L) because  $\phi_m = 0.42$  is located in a more retarded CA50 range. This observation is important to explain the different trends in  $\eta_{\text{th}}$  between  $\phi_m = 0.32$  and 0.42, as summarized below.

#### Summary of the Effect of CA50 and Knock on the $\eta_{\text{th}}$

At a given  $\phi_m$ , when CA50 is advanced from a highly retarded point, there is a tradeoff between the improved expansion ratio increasing the  $\eta_{\text{th}}$  and increased HT reducing  $\eta_{\text{th}}$ . Once knock occurs, the HT-coefficient increases rapidly and was found to be the dominant effect in explaining the greater increase in the HT.

For  $\phi_m = 0.32$  and 0.42, the  $\eta_{\text{th}}$  initially increases in the non-knocking region mainly because of a more advanced CA50 which improves the expansion efficiency and to a smaller extent because of better  $\eta_{\text{comb}}$ . This dominates the slight increase in the HT due to a more advanced CA50. However, as CA50 is further advanced, the RI eventually increases to the point that acoustic oscillations become sufficiently strong (above  $RI \approx 5 \text{ MW/m}^2$ ) to cause a large increase in the HT-coefficient. For lower  $\phi_m$  of 0.32, in CA50 range close to TDC, the

decreasing benefits of both, the higher  $\eta_{\text{comb}}$  and the better expansion ratio do not compensate anymore for the faster increase in the HT. Therefore, the  $\eta_{\text{th}}$  drops as CA50 is further advanced from the knock onset point. For the higher  $\phi_m$  of 0.42, because the CA50 range is overall more retarded (for a given variation in RI), advancing the CA50 in the knock region still results in higher  $\eta_{\text{th}}$  because of the still significant gain in expansion ratio. However the rate of increase in the  $\eta_{\text{th}}$  decreases primary due to the enhancement of the HT caused by knock effects. These higher efficiency operating points are not considered as acceptable owing to emission of the irritating sound of knock. It is worth mentioning that apart from the increase in knock noise intensity (for RI > 5 MW/m<sup>2</sup>), the “base” noise induced by the normal combustion event, not as irritating as the knock noise, also increases with CA50 being more advanced. This “base” noise is characterized by the CNL [20] and correlates with higher PPRR [20]. For  $\phi_m = 0.42$ , at a RI of 5 MW/m<sup>2</sup>, the CNL is 90 dB. At RI  $\approx$  14 MW/m<sup>2</sup>, the base noise has increased substantially to 95.8 dB, in addition to the irritating sound of knock.

The decrease in the EGR rate required to achieve a more advanced CA50 for this constant  $T_{\text{in}}$  sweep does not significantly affect  $\gamma$ . This is because the lower EGR rate (less triatomic molecules) is compensated by higher combustion temperatures with more advanced CA50.

Overall, for higher  $\eta_{\text{th}}$  (and also  $\eta_{\text{comb}}$ ), it is desirable to advance the CA50 as much as possible toward TDC, with the constraint RI  $\leq$  5 MW/m<sup>2</sup> to prevent onset of knock. However for operating points with relatively good  $\eta_{\text{comb}}$  (above 96% according to [4]), even without knock, there is typically little potential benefit in advancing the CA50 beyond about 366-368°C, as shown in [4, 6]. This is due to the decreasing gain in expansion ratio as CA50 approaches TDC compared to the increase in the HT (even in the non-knocking region). For more retarded / higher- $\phi_m$  points, advancing CA50 offers significant potential for improving  $\eta_{\text{th}}$ . One method demonstrated to achieve this without knock is by using Partial Fuel Stratification (PFS) [2, 4, 14].

## ***Influence of $\phi_m$ at Constant RI = 5 MW/m<sup>2</sup> on the Energy Distribution***

### ***Introduction of the Operating Conditions and Energy Distribution***

At a given  $P_{\text{in}}$ , a practical method to increase load without knock and with good stability<sup>12</sup> while maximizing the  $\eta_{\text{th}}$  is to progressively increase  $\phi_m$  at the RI threshold for knock (RI = 5 MW/m<sup>2</sup> in our case). In this way, the CA50 is the most advanced (after TDC) to benefit from the highest expansion ratio for acceptable operation as seen in the previous section.

In the following case, at a boost pressure of 2.4 bar,  $\phi_m$  is swept with  $T_{\text{in}}$  held constant at 30°C, the lowest practical  $T_{\text{in}}$  achievable with our facility. In contrast to the previous section for which the fuel was fully PM, early-DI fueling was used. With DI, although the mixture is overall well-mixed because of the early injection (60°C), some mixture stratification remains up to the start of the combustion [4]. At this  $P_{\text{in}}$ , gasoline becomes  $\phi$ -sensitive. Thus, the mixture stratification

<sup>12</sup> For information about how stability varies for our engine as conditions are changed, please refer to refs. [13, 14, 36, 37]. Our acceptable limit is set at 2% of the standard deviation of the IMEP<sub>g</sub>. For the  $\phi_m$  / CA50 sweep presented in the following, the standard deviation of IMEP<sub>g</sub> never exceeds 1%.

acts to stage the combustion and the HRR is reduced which allow more CA50 advancement compare to fully PM, before knock occurs [14]. Therefore, because of this effect, higher  $\eta_{\text{th}}$  is achieved for the same RI (or alternatively higher  $\phi_m$  without knock for the same CA50) [4]. The possibility to use lower  $T_{\text{in}}$  with DI compared to PM also improve the  $\eta_{\text{th}}$ , as it will be shown in the next section. For these tests, with higher- $\phi_m$ , the CA50 needs to be retarded (Figure 11a) to prevent knock. Reasons for the need to retard the CA50 with increased  $\phi_m$  are explained in details in [17]. The CA50-retard has been carried out by progressively adding more EGR and holding the RI at  $\sim$  5 MW/m<sup>2</sup>. Experimental conditions for this sweep are summarized in Table 4.

**Table 4: Operating conditions for the  $\phi_m$  effect (at constant RI) on the  $\eta_{\text{th}}$ .**

<b>Geometric CR [-]</b>	16:1
<b>Engine speed [RPM]</b>	1200
<b><math>P_{\text{in}}</math> [bar] (+/- 0.01 bar)</b>	2.4
<b><math>T_{\text{in}}</math> [°C] (+/- 1°C)</b>	30
<b><math>\phi_m</math> [-]</b>	0.26 → 0.40
<b>RI [MW/m<sup>2</sup>] (+/- 0.3 MW/m<sup>2</sup>)</b>	5
<b>O<sub>2</sub>-intake [%<sub>vol</sub>]</b>	18.5 → 11.2
<b>IMEP<sub>g</sub> [bar]</b>	9.4 → 14.3
<b>Fuel</b>	Certification gasoline
<b>Fueling strategy</b>	GDI with SOI @ 60°C

As  $\phi_m$  increases, as seen in Figure 11b, the  $\eta_{\text{th}}$  increases through a maximum of  $\sim$  49.3% at about  $\phi_m \approx$  0.29. Then, the  $\eta_{\text{th}}$  gradually decreases. Meanwhile, the  $\eta_{\text{comb}}$  continuously increases primary because of higher combustion and wall temperatures [4, 13]. The increase in the EGR rate with higher  $\phi_m$  (not shown) also contributes to higher  $\eta_{\text{comb}}$  by giving a second chance for unburned-HC and CO to burn [13]. For  $\eta_{\text{comb}}$  above  $\sim$  97.5%, the slope of the  $\eta_{\text{comb}}$ -curve decreases. This characteristic is important regarding the trend in  $\eta_{\text{th}}$ , as it is explained in the following. Also shown in Figure 11b (open symbol) is the hypothetical change in  $\eta_{\text{th}}$  considering only the effect of the increased  $\eta_{\text{comb}}$  relative to the lowest  $\phi_m$  point. As can be seen, this curve matches almost exactly with the rapid increase in measured  $\eta_{\text{th}}$  up to the maximum  $\eta_{\text{th}}$  point ( $\phi_m = 0.29$ ). In agreement with [4], the  $\eta_{\text{comb}}$  is a key factor affecting the  $\eta_{\text{th}}$ , towards low- $\phi_m$ . Then, for  $\phi_m$  above 0.29, the  $\eta_{\text{th}}$  drops despite the still increasing  $\eta_{\text{comb}}$  (however at a lower rate). The decreasing trend in  $\eta_{\text{th}}$  is known to be significantly affected by the lower expansion ratio with the more retarded CA50, particularly beyond 366°C [4], which is the case here. The higher EGR rate and higher combustion temperatures resulting from the higher  $\phi_m$  also reduce  $\gamma$  of the charge and therefore act to lower the  $\eta_{\text{th}}$ . However, as stated in [4], the effect of  $\gamma$  is thought to be secondary in comparison to the changes in expansion ratio.

Overall, the reason for the trend in  $\eta_{\text{th}}$  can be fairly well explained by only considering the tradeoff between  $\eta_{\text{comb}}$  and expansion ratio +  $\gamma$ . The  $\eta_{\text{th}}$  initially increases as  $\phi_m$  is increased, because of the rapid increase in  $\eta_{\text{comb}}$ . In this corresponding CA50 range, the expansion ratio is not significantly altered. However, above  $\phi_m$  of 0.29, the  $\eta_{\text{th}}$  decreases because of the reduced expansion ratio combined with the lower  $\gamma$ . This effect is not compensated by the improvement in  $\eta_{\text{comb}}$

which diminishes above  $\phi_m$  of 0.29. However, actual effects are more complex and thus it is of interest to better quantify the relative effects of  $\gamma$  compared to the expansion ratio. It is also unclear how the HT and Exh-L vary through such a  $\phi_m$  sweep.

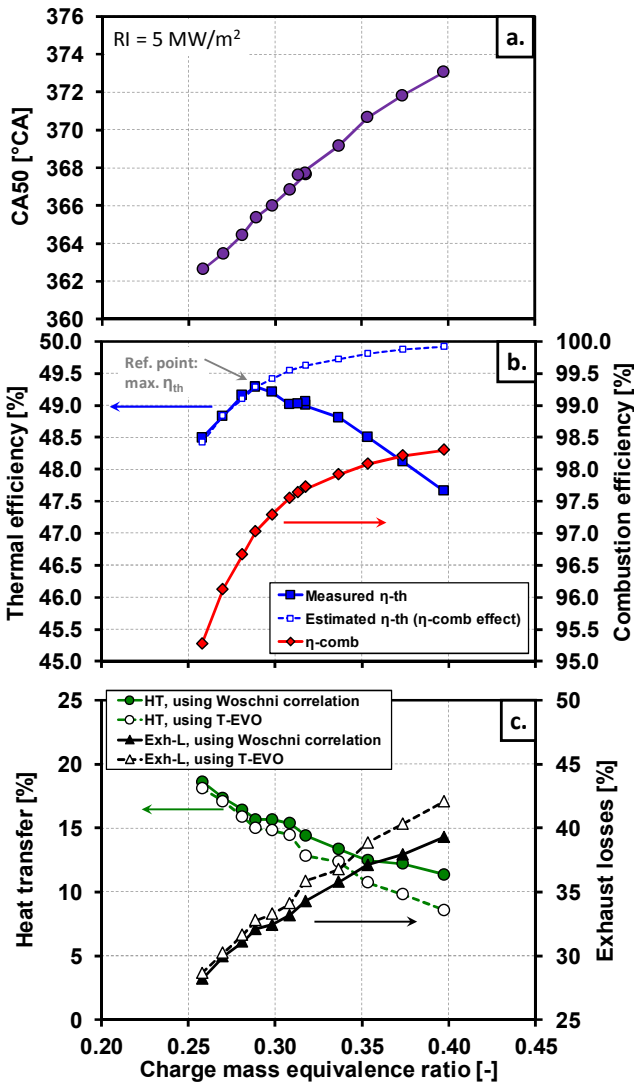


Figure 11: Variation of CA50 (a.) and energy distribution across the  $\phi_m$  sweep at RI = 5 MW/m<sup>2</sup> (b.):  $\eta_{th}$  and  $\eta_{comb}$ . Estimated- $\eta_{th}$  shows the trend in  $\eta_{th}$  from the reference point indicated in the plot by only considering the change in  $\eta_{comb}$  (c.): HT and Exh-L estimated with two different methods. See Table 4 for operating conditions.

Referring to Figure 11c, the fraction of energy lost through HT significantly decreases ( $\sim 7.0\%$ -units according to the Voschni analysis) as  $\phi_m$  is increased over the sweep. This trend is somewhat unexpected, knowing that combustion temperatures are higher, which causes an increase in  $\Delta T$  with increased  $\phi_m$  as shown in Figure 12b. The higher  $\Delta T$  would tend to enhance the HT. It is important to mention the good agreement between the trends provided by either directly computing the HT using the Voschni correlation or indirectly through the calculation of the internal energy in the exhaust (using  $T_{EVO}$ ) and applying the energy balance equation to obtain the HT. This agreement gives confidence that the captured trend of lower HT with increased  $\phi_m$  for constant RI = 5 MW/m<sup>2</sup> is correct. This behavior was also mentioned by Saxena and Bedoya [6].

Understanding it requires further analysis which is provided in the next subsection. Nonetheless, this significant decrease in the HT tends to increase the  $\eta_{th}$  across the load range. Therefore, it should be considered in the tradeoff for a full explanation of the variation in  $\eta_{th}$ .

In parallel, Figure 11c also shows that the Exh-L increases, at a higher rate than the HT decreases ( $\sim 10.8\%$ -units for the Exh-L vs.  $\sim 7.0\%$ -units for the HT across the  $\phi_m$ -range, according to the Voschni analysis). Details explaining these trends and its impact on the  $\eta_{th}$  are provided in the next subsection.

### Insight into HT and Exh-L

Figure 12 presents (a) HT-rate traces, (b)  $\Delta T$ , and (c) the HT-coefficient (derived with the Voschni correlation) for four selected  $\phi_m$ . As can be seen, when  $\phi_m$  is increased, even though the peak- $\Delta T$  rises, the peak-HT-rate decreases. This is due to a significant decrease in the HT-coefficient during the combustion event. Reasons for this phenomenon are not well understood and a fundamental research study into HT exchange processes would be required, which is beyond the scope of this study. Nevertheless, it could be hypothesized that the turbulent flow structures responsible for the HT are produced mainly by flows during the intake stroke and become more dissipated as CA50 is retarded. Appendix 1 provides evidence that CA50 is a more fundamental parameter affecting the HT, than the effect of  $\phi_m$ .

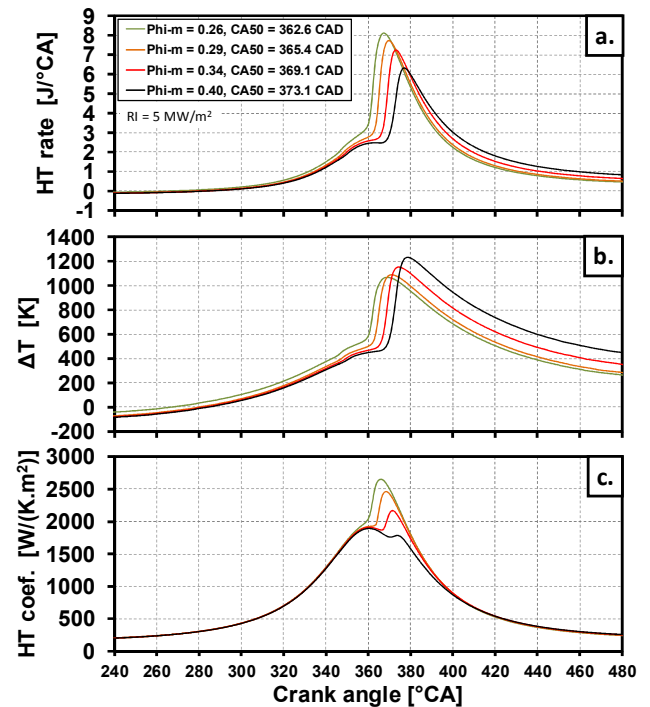


Figure 12:  $\phi_m$  effect at RI = 5 MW/m<sup>2</sup> on the HT rate (a.), the  $\Delta T$  (b.) and the HT coefficient (c.) evaluated using the Voschni correlation. See Table 4 for operating conditions.

During the compression stroke, the HT-rate also decreases with increased  $\phi_m$  (Figure 12a), however at a lesser degree than during combustion. This is due to the lower  $\Delta T$  because of hotter walls as  $\phi_m$  is increased, and because of the lower compressed gas temperatures due to lower  $\gamma$  with more fuel and EGR. Note that during this period, the HT-coefficient remains unchanged. The opposite occurs during

the expansion stroke beyond  $\sim 400^\circ\text{CA}$ , with the HT-rate increasing with increased  $\phi_m$  due to higher in-cylinder temperatures (higher  $\Delta T$ , Figure 12b) and similar HT-coefficients. Interestingly, the absolute amount of energy lost through HT (*i.e.* integration of the HT-rate in Figure 12a) is quasi-constant over this  $\phi_m$  sweep: the lower HT-rate during compression and combustion with increased  $\phi_m$  is balanced by higher HT-rate during expansion. Because the amount of fuel supplied increases significantly over the sweep, the HT as percentage of supplied fuel energy decreases as shown in Figure 11c and discussed previously.

Figure 13 presents a detailed decomposition of the factors contributing to the variation of the Exh-L for this  $\phi_m$  sweep. Note that this graph is plotted as a function of CA50 which increases with increased  $\phi_m$  as shown in Figure 11a. As seen by the red curve in Figure 13, the increase in the  $\eta_{\text{comb}}$  by about 3% (Figure 11b) acts to increase the Exh-L by slightly more than 1%, because the Exh-L represents  $\sim 1/3$  of the total energy (Figure 11c). Also, across this  $\phi_m$  / CA50 sweep, a significant fraction of the decrease in the HT (Figure 11c) cannot be recovered as useful work and contributes to higher Exh-L (blue curve in Figure 13). However, the increase in the Exh-L due to the better  $\eta_{\text{comb}}$  and lower HT does not directly impede the  $\eta_{\text{th}}$ . Indeed, a larger fraction of the increase in the  $\eta_{\text{comb}}$  and decrease in the HT acts to increase the  $\eta_{\text{th}}$  than is lost into the exhaust. In this case,  $\sim 50\%$  of the increase in  $\eta_{\text{comb}}$ , and  $\sim 60\%$  of the decrease in HT act to increase the  $\eta_{\text{th}}$ .

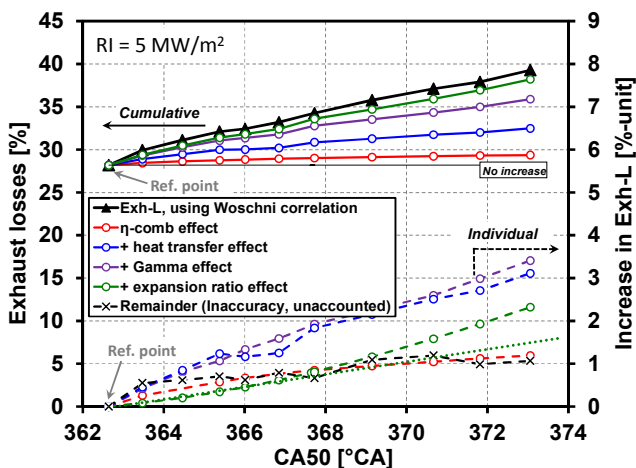


Figure 13: Detailed effect of  $\phi_m$  on the Exh-L as a function of CA50 at constant RI = 5 MW/m<sup>2</sup>. Individual and cumulated contributions of  $\eta_{\text{comb}}$ , HT, expansion ratio and  $\gamma$  are shown from a reference point. See Table 3 for operating conditions.

Changes in  $\gamma$  and the effective expansion ratio over the sweep directly affect the  $\eta_{\text{th}}$  and Exh-L. A linear regression fitted on the most advanced points (low  $\phi_m$ ) of the individual effect of the “expansion ratio” curve (thin green dotted-line in Figure 13) shows a deviation from the curve beyond  $\sim 368^\circ\text{CA}$ . This deviation reflects the greater change in expansion ratio as CA50 shifts farther from TDC due to the kinematics of the piston assembly, as also shown in [6].

It is interesting to notice that for this sweep, the effect of  $\gamma$  is among the most important contributors to increase the Exh-L. Thus, it is the main reason why the  $\eta_{\text{th}}$  drops for  $\phi_m$  above  $\sim 0.30$  (CA50 = 366°CA) with the expansion ratio being almost as strong. As mentioned before,  $\gamma$  of the expanding gas decreases with  $\phi_m$  because of the higher

combustion temperatures, higher EGR-rate and also due to the increase in the supplied fuel mass (more tri-atomic molecules).

Finally, by adding-up the contributions of each individual effect, a relatively good closure is achieved with a remainder of about 1% at most.

### Summary of the Effect of $\phi_m$ on the $\eta_{\text{th}}$

Increasing  $\phi_m$  at constant RI yields to a significant decrease in the HT. This trend is somewhat unexpected, because higher  $\phi_m$  produces higher  $\Delta T$  which should act to increase the HT. The lower HT is attributed to the progressive drop of the HT-coefficient during the combustion event as CA50 is retarded to prevent knock when  $\phi_m$  is increased.

The trends in the different factors described above help to better understand the tradeoff affecting the  $\eta_{\text{th}}$  when  $\phi_m$  is increased. The increase in the  $\eta_{\text{comb}}$  and the decrease in the HT (with CA50 retard) act to increase the  $\eta_{\text{th}}$ . The lower expansion ratio together with a decrease in  $\gamma$  hurt the expansion efficiency and thus tend to decrease the  $\eta_{\text{th}}$ .

For relatively low- $\phi_m$  (0.26 to 0.30), the increase in the  $\eta_{\text{th}}$  has been found to correlate well with the expected effect of the increase in the  $\eta_{\text{comb}}$ . For this engine speed and boost pressure, at low- $\phi_m$ , the relatively poor  $\eta_{\text{comb}}$  is considered to be the parameter that most impedes the  $\eta_{\text{th}}$ . As shown by Aceves *et al.* [38], as  $\phi_m$  is reduced below the value that induces a fast drop of the  $\eta_{\text{comb}}$ , incomplete combustion zones are located near the walls due to a broadening of the boundary layer where the temperature is not high enough (below 1500 K [7-9]). In the background, although the effect of a change in the expansion ratio is small, it is still present as shown in Figure 13 and tends to slightly reduce the  $\eta_{\text{th}}$  as CA50 is delayed. In addition,  $\gamma$  of the charge decreases. However, both of these effects (expansion ratio and  $\gamma$ ) must be canceled by the decrease in the HT so that only the magnitude of the change in  $\eta_{\text{comb}}$  explains the variation in  $\eta_{\text{th}}$ .

For higher  $\phi_m$  ( $> \sim 0.30$ ), the  $\eta_{\text{th}}$  decreases because of the still increasing Exh-L due to  $\gamma$ -effect and due to the growing magnitude of the losses caused by the lower expansion ratio. These are not compensated anymore by the decrease in the HT and the diminishing improvement in  $\eta_{\text{comb}}$ .

A key finding is that, unlike the effect of varying CA50 alone (see previous section), the decrease in  $\gamma$  appears to be the largest contributor to the decrease in the  $\eta_{\text{th}}$  as CA50 is delayed with increased  $\phi_m$  for constant RI. It is followed by the growing magnitude of the losses due to lower effective expansion ratio with more CA50 retard, but they do not dominate over the  $\gamma$ -effect in the CA50-range considered. These effects are mitigated by the decreased HT. Finally, just as for the CA50 sweep, there is potential for increasing the  $\eta_{\text{th}}$  in the highest- $\phi_m$  region (which are more retarded) by applying a higher degree of PFS than this early DI, that allows CA50 to be more advanced at constant RI.

## Influence of $T_{in}$ on the Energy Distribution

### Introduction of the Operating Conditions and Trends in $\eta_{th}$

$T_{in}$  is an important control variable to achieve autoignition at the desired CA. To maximize the IMEP<sub>g</sub> at a given  $\phi_m$  and  $P_{in}$ , using the lowest possible  $T_{in}$  is desirable because of the higher charge density [39]. With the use of intake boost to achieve higher loads, the enhancement of autoignition by the increased pressure can become so strong that  $T_{in}$  would have to be reduced to temperatures below 30°C, which is not practical, so variable amounts of EGR are commonly used instead [13]. Reducing  $T_{in}$  has also been shown to improve the  $\eta_{th}$  [4]. The efficiency improvements were attributed to 1) the better  $\gamma$  because of the lower temperature and because less EGR is required to control CA50, and 2) an assumed reduction in HT due to lower compressed-gas and combustion temperatures. However, ref. [4] pointed out the need to better characterized the relative importance between these two factors.

In this study,  $T_{in}$  has been varied between 30°C and up to 70°C in 10°C increments. In order to assess the  $\phi_m$ -value for maximum- $\eta_{th}$  as  $T_{in}$  varies, a  $\phi_m$ -sweep has been conducted for each  $T_{in}$ , in the range around the maximum  $\eta_{th}$ . The RI was maintained at  $\sim 5$  MW/m<sup>2</sup> by using EGR to control the CA50. Consistently, more EGR is needed for higher  $T_{in}$  (as indicated by the reduced O<sub>2</sub> concentration in the intake, Table 5). For  $T_{in} = 30^\circ\text{C}$ , operating conditions are the same as the  $\phi_m$ -sweep analyzed in the previous section. Comparing the  $\eta_{th}$  in Figure 11a with the curve at 30°C in Figure 14b reveals that the  $\eta_{th}$  is very repeatable, within  $\pm 0.2\%$ -unit. This repeatability is of primary importance here, in order to properly detect the relatively small effect of  $T_{in}$  on the  $\eta_{th}$ , within a reasonable range of  $T_{in}$ .

Table 5: Operating conditions for the  $T_{in}$  effect (at constant RI) on the  $\eta_{th}$ .

Geometric CR [-]	16:1				
Engine speed [RPM]	1200				
$P_{in}$ [bar] (+/- 0.01 bar)	2.4				
$T_{in}$ [°C] (+/- 1°C)	30	40	50	60	70
RI [MW/m <sup>2</sup> ] (+/- 0.3 MW/m <sup>2</sup> )	$\sim 5$				
$\phi_m$ [-]	0.30				
O <sub>2</sub> -intake [% <sub>vol.</sub> ]	14.8	13.9	13.3	12.7	12.1
IMEP <sub>g</sub> [bar]	11.0	10.8	10.6	10.3	10.1
Fuel	Certification gasoline				
Fueling strategy	GDI with SOI @ 60°C				

In Figure 14a, it can be noticed that over the  $\phi_m$ -range investigated, there is a negligible change in CA50 for the different  $T_{in}$ . At  $T_{in} = 30^\circ\text{C}$ , the CA50 is a little more advanced than for the other  $T_{in}$ . Multiple repetitions of such a sweep at the same conditions indicate that this difference is somewhat in the noise / repeatability of the test. This quasi-similar CA50 means that the  $\eta_{th}$  would not be significantly altered by the small changes in the effective expansion ratio.

According to Figure 14b, for  $T_{in} = 30$  and 40°C, the  $\eta_{th}$  curves overlap. Multiple repetitions of the tests at these two  $T_{in}$  indicate that this behavior is consistent. Then, as  $T_{in}$  is further increased, the  $\eta_{th}$

gradually decreases ( $\sim -0.25\%$ -unit / 10°C). Meanwhile, the  $\eta_{comb}$  consistently increases (Figure 14b). An increase in  $\eta_{comb}$  with higher  $T_{in}$  is believed to be mainly due to the use of more EGR by offering a second chance to the HC and CO in the EGR to burn, as explained in details in ref. [13].

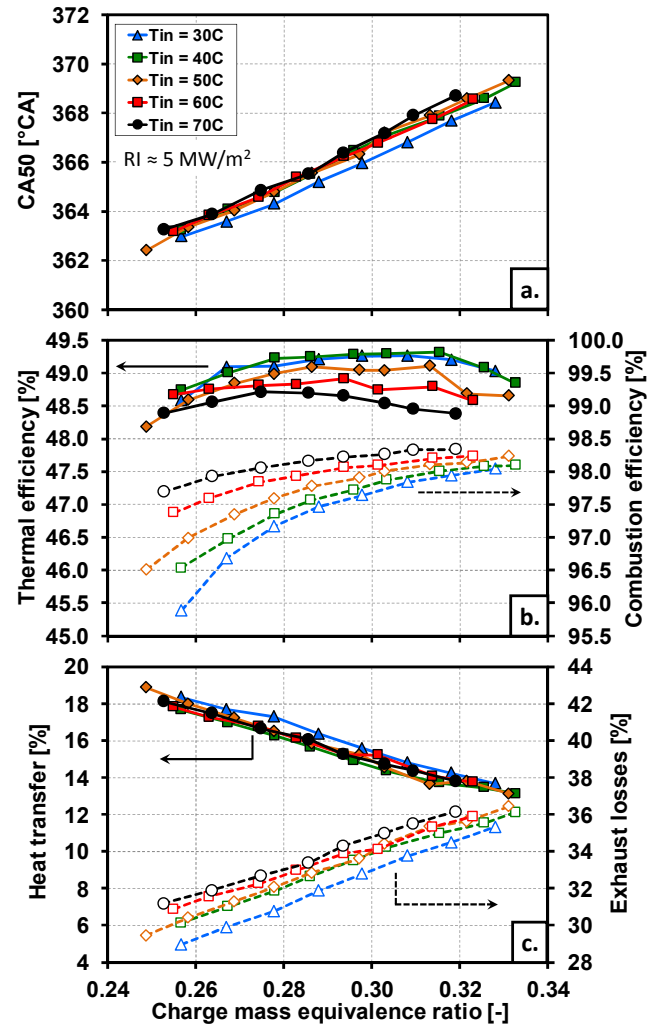


Figure 14: Variation of CA50 (a.) and energy distribution for  $\phi_m$  sweeps at different  $T_{in}$  and  $RI \approx 5$  MW/m<sup>2</sup>; (b.):  $\eta_{th}$  and  $\eta_{comb}$ . (c.): HT and Exh-L derived from the use of the Woschni correlation. See Table 5 for operating conditions.

### Insight into the HT and Exh-L

Analysis of the Figure 14c reveals that a change in  $T_{in}$  between 30°C and 70°C does not cause a variation in the HT significant enough to explain the observed decrease in  $\eta_{th}$ . As can be seen, between 40°C and 70°C, the HT curves overlap. The slightly higher HT for  $T_{in} = 30^\circ\text{C}$  correlates with the more advanced CA50 (Figure 14a). Indeed, as shown in Appendix 1, Figure 21 (scenario #2), these same curves collapse within  $\pm 0.5\%$ -unit, when they are replotted against CA50.

These results are in disagreement with what was hypothesized in a previous study [4], that the HT would be enhanced with higher  $T_{in}$  due to higher compressed-gas and combustion temperatures. However, according to Figure 15a, the HT-rate during the combustion event decreases with higher  $T_{in}$ , owing to a lower HT-

coefficient (Figure 15c). Note that the change in the gas-wall temperature difference ( $\Delta T$ ) (Figure 15b) seems to be small during combustion and expansion for the various  $T_{in}$ . Although a physical explanation is missing concerning the decrease in the HT-coefficient during combustion, it seems that the reduced HT-rate with increased  $T_{in}$  scales with the lower HRR / lower combustion-induced pressure rise, so that the total-HT normalized by the total supplied energy in Figure 14c is insensitive to changes in  $T_{in}$ <sup>13</sup>.

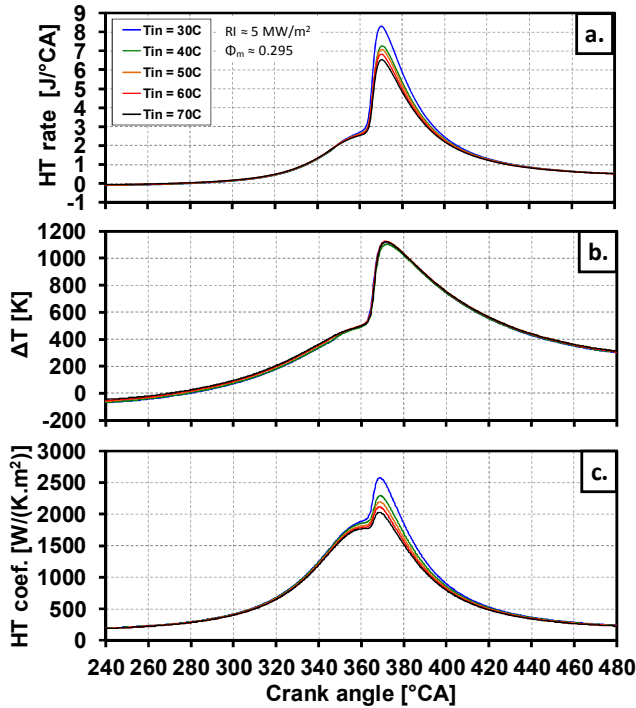


Figure 15:  $T_{in}$  effect at  $\phi_m \approx 0.295$  and  $RI \approx 5 \text{ MW/m}^2$  on the HT rate (a.), the  $\Delta T$  (b.), and the HT coefficient (c.), obtained from using the Woschni correlation. See Table 5 for operating conditions.

Applying the energy balance equation to compute Exh-L (Eq. 6), the Exh-L logically increases (Figure 14c) in order to take into account of the lower  $\eta_{th}$ , as well as to compensate for the higher  $\eta_{comb}$ . A detailed analysis of the Exh-L is presented in Figure 16. The increase in the Exh-L with  $T_{in}$  (black continuous line with triangle symbols) is given for a  $\phi_m$  of 0.30, derived by interpolating the data in Figure 14. It can be seen that the effects of change in  $\eta_{comb}$ , expansion ratio and HT are small and/or in the noise in the data. Of particular interest is the significant increase in the Exh-L due to a change in  $\gamma$  with higher  $T_{in}$  (purple curve).  $\gamma$  decreases because the gas temperature over the cycle slightly increases with higher  $T_{in}$ , but the main factor is attributed to the greater amount of EGR required to maintain  $RI \approx 5 \text{ MW/m}^2$ . This is likely to be the most pertinent factor impeding the  $\eta_{th}$  as  $T_{in}$  is increased. The relatively good closure of the Exh-L depicted in Figure 16 (remainder  $\approx 0.5\%$  maximum) gives confidence that the right cause for the decrease in  $\eta_{th}$  has been identified.

<sup>13</sup> As  $T_{in}$  increases, the total supplied energy decreases by the same amount as the decrease in the absolute-HT, so that the fraction of energy lost by HT is insensitive to a change in  $T_{in}$ , at least in the 30 to 70°C-range investigated here. As a reminder, the total supplied energy decreases because of the reduced charge density with higher  $T_{in}$  at constant  $P_{in}$  and  $\phi_m$ .

Finally, these data show that decreasing the  $T_{in}$  from 40°C to 30°C does not provide any gain in  $\eta_{th}$  (Figure 14a). The cause(s) for this limitation are difficult to identify because of the very small differences of the different factors that affect  $\eta_{th}$ . Nevertheless, in Appendix 3, the data are scrutinized further and a plausible reason for this is presented.

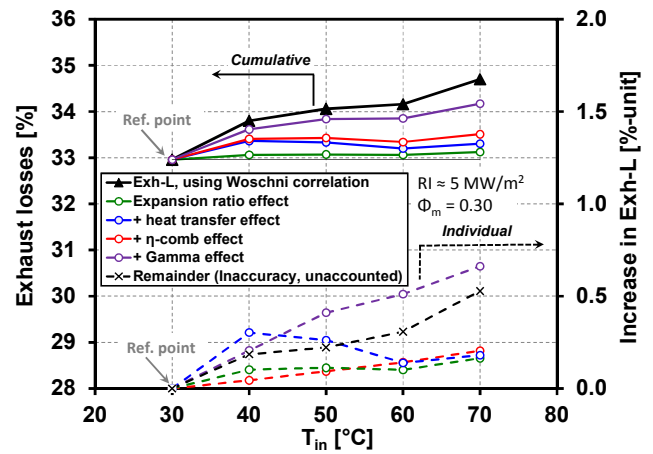


Figure 16: Detailed effect of  $T_{in}$  on the Exh-L interpolated at  $\phi_m = 0.30$  and for  $RI \approx 5 \text{ MW/m}^2$ . Individual and cumulated contributions of  $\eta_{comb}$ , HT, expansion ratio and  $\gamma$  are shown from a reference point. See Table 5 for operating conditions.

#### Summary of the Effect of $T_{in}$ on the $\eta_{th}$

These results show that under moderately boosted conditions (*i.e.* 2.4 bar absolute) and at 1200 RPM,  $T_{in} = 40^\circ\text{C}$  was found to be an appropriate  $T_{in}$  to maximize  $\eta_{th}$ . This temperature should be achievable with current intercoolers of turbo-charged engines. If the emissions of HC and CO are an issue, higher  $T_{in}$  can be used to improve  $\eta_{comb}$ . The increase in the  $\eta_{comb}$  with higher  $T_{in}$  is mainly related to the fact that more EGR is needed (re-burn of HC and CO in EGR). However, at fixed  $\phi_m$ , increasing  $T_{in}$  will be accompanied with a commensurate penalty in IMEP due to the reduced charge-density and slightly decreased- $\eta_{th}$ . If  $\phi_m$  is increased to keep the IMEP the same, as seen in the previous section, the need to delay the CA50 will further decrease the  $\eta_{th}$ . At constant  $\phi_m$ , the slight decrease in the  $\eta_{th}$  as  $T_{in}$  is increased is caused by a lower  $\gamma$ , while CA50 and HT have virtually no effect.

#### Influence of Engine Speed

##### Introduction of the Operating Conditions and Energy Distribution

From our baseline conditions (1200 RPM,  $P_{in} = 2.40 \text{ bar}$ , 100% DI @ 60°CA,  $RI \approx 5 \text{ MW/m}^2$ ) and an optimized  $T_{in}$  of 40°C, engine speed was swept down to 1000 RPM and up to 2000 RPM. For each speed, a  $\phi_m$ -sweep was conducted between  $\sim 0.27$  and  $\sim 0.34$  to ensure that the data covered the maximum  $\eta_{th}$  range. Similar to the  $T_{in}$  sweep in Figure 14,  $\eta_{th}$  showed little variation with  $\phi_m$  near the peak. Results are only presented for a  $\phi_m$  of 0.30 by interpolating the corresponding trends provided in Appendix 4. With a constant  $T_{in} = 40^\circ\text{C}$ ,  $RI$  of  $\sim 5 \text{ MW/m}^2$  is maintained by using EGR to control the CA50 as  $\phi_m$  and engine speed are varied. Experimental conditions are only shown for a  $\phi_m$  of 0.30 in Table 6.

Table 6: Operating conditions shown for a  $\phi_m = 0.30$ , for the engine speed effect (at constant RI) on the  $\eta_{th}$ .

Geometric CR [-]	16:1						
Engine speed [RPM]	1000	1200	1300	1400	1600	1800	2000
$P_{in}$ [bar]	2.4						
$T_{in}$ [°C]	40						
RI [MW/m <sup>2</sup> ]	~ 5						
$\phi_m$ [-]	0.30						
O <sub>2</sub> -intake [% <sub>vol.</sub> ]	13.1	14.3	14.6	15.2	16.2	17.1	18.2
IMEP <sub>g</sub> [bar]	10.6	10.9	11.0	10.8	10.8	10.6	10.3
Fuel	Certification gasoline						
Fueling strategy	GDI with SOI @ 60°CA						

Figure 17 shows the main results. As speed is increased, CA50 must be retarded to maintain a RI of ~ 5 MW/m<sup>2</sup> (Figure 17a). Therefore, this acts to reduce the  $\eta_{th}$  because of the lower expansion ratio. This effect is greater for the higher speeds due to the greater change in expansion ratio per CA-degree at later CA50. As seen in Figure 17b, the  $\eta_{th}$  peaks at about 49.4% and is fairly constant (within the accuracy of the measurements) between 1200 and 1600 RPM. Above and below that speed range, the  $\eta_{th}$  decreases. The  $\eta_{comb}$  decreases when engine speed is increased for this constant  $\phi_m$  (Figure 17b). This happens because of the reduced time for oxidation with increased speed and because of the lower peak-temperature with more retarded CA50 [9]. As seen in Figure 17b, the effects of the changes in  $\eta_{comb}$  explain a large part of the change in  $\eta_{th}$ . However, HT,  $\gamma$  and expansion ratio must also be considered.

This trend in  $\eta_{th}$  with engine speed is very similar to the ones reported in ref. [4] for a smaller speed range. In ref. [4], it was argued that the HT should consistently decrease with increased speed due to the reduced time for HT. As shown in Figure 17c, the HT first decreases from 1000 to about 1300 RPM, as expected. This initial decrease in the HT correlates well with the increase in  $\eta_{th}$  from 1000 to 1200/1300 RPM. However, the HT becomes quasi-constant up to 2000 RPM. Reasons for this behavior are explained in the next subsection.

### Insight into the HT and Exh-L

According to Figure 18a, the HT during the compression stroke consistently decreases with increased speed, in spite of a slightly higher  $\Delta T$  (Figure 18b) and higher HT-coefficient (Figure 18c). The higher velocity of the intake gas with increased speed creates higher in-cylinder turbulence which is responsible for the increase in the HT-coefficient by 25% from 1000 to 2000 RPM. The dissipation of these turbulent eddies leads to higher charge-gas temperatures [32]. However, the higher HT-coefficient is overtaken by the reduced time for HT with increased speed so that the HT-rate during the compression stroke decreases. This is taken into account in Equation 6 with the normalization by the time scale (*i.e.* 1/engine speed, converting [W] to [J]).

During the combustion event, a non-monotonic behavior in the HT-rate with engine speed can be observed. First, the HT-rate decreases from 1000 to 1300 RPM, also due to the reduced time for HT. Then, the HT-rate increases very rapidly for higher engine speeds (except at 2000 RPM). As seen in Figure 18c, this is attributed to the rapid

increase in the HT-coefficient for speeds above 1300 RPM which now dominates over the reduced-time for HT. This behavior only appears during the combustion event which strongly suggests that this is induced by a combustion-related phenomenon, and particularly the onset of knock as explained in the following.

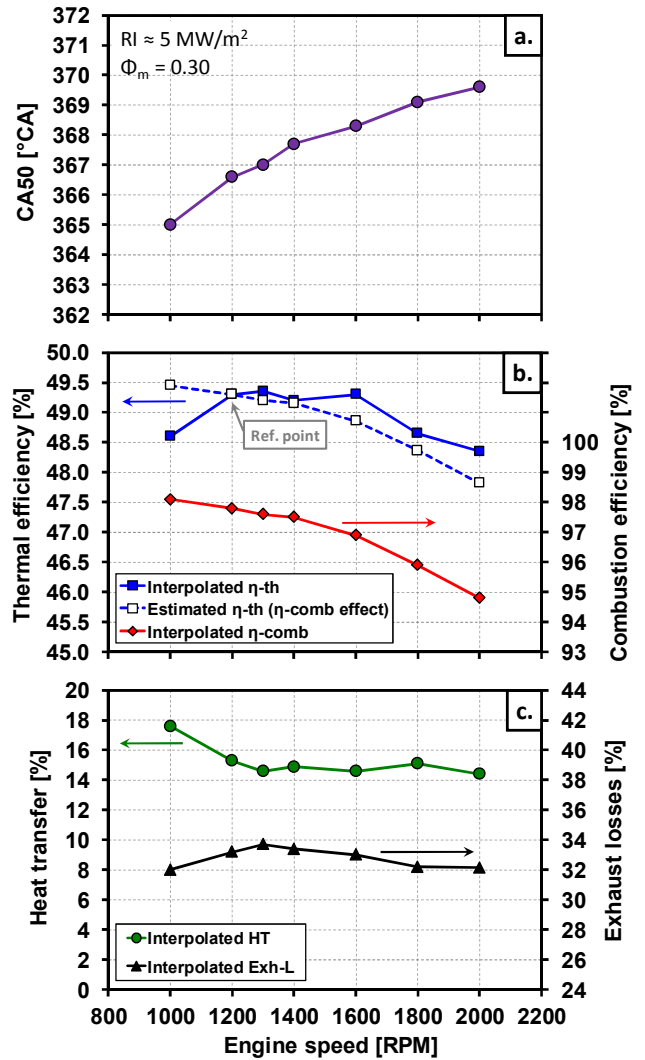


Figure 17: Engine speed effect at  $\phi_m = 0.30$  and  $RI \approx 5 \text{ MW/m}^2$  on the HT rate (a.), the  $\Delta T$  (b.), and the HT coefficient (c.), obtained from using the Woschni correlation. See Table 6 for operating conditions.

In a previous study dealing with noise in LTGC engines [20], evidence was provided showing that the RI correlation might not accurately indicate the onset of knock for large changes in engine speeds. In particular, the amplitude of the ripples on the pressure trace was seen to increase significantly as speed was increased at constant RI from 1200 to 2400 RPM. The same behavior was observed for the sweep of the current study. Moreover, as shown in the first part of the results section (CA50 effect), the onset of knock is characterized by a rapid increase in the HT-rate during the combustion event. Additionally, the onset of knock was found to correlate well with  $C_2$  (Figure 7). Figure 19 shows similar characteristics to the  $\phi_m = 0.32$  data in Figure 7: a well-defined change in the slope in KI and  $C_2$ . This means that even though RI was maintained at 5 MW/m<sup>2</sup> over this speed sweep, the magnitude of acoustic oscillations, represented by KI, as well as influence on the

combustion-induced HT (*i.e.*  $C_2$ ) increase substantially for speeds above 1300-1400 RPM. Consequently, the onset of strong acoustic oscillations (*i.e.* knock) is the most likely reason to explain the increase in the HT-rate during the combustion event above 1300 RPM. It overcomes the effect of reduced-time for HT. However, the increase in the HT-rate during combustion due to knock is compensated by the decrease in the HT-rate during the compression stroke, so that the total in HT in Figure 17b is nearly constant from 1300 to 2000 RPM.

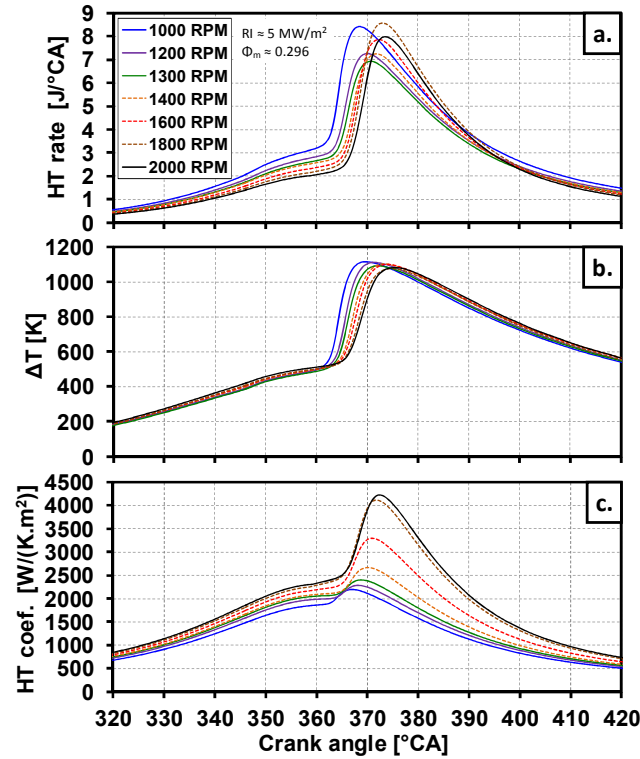


Figure 18: Engine speed effect at  $\phi_m \approx 0.296$  and  $RI \approx 5 \text{ MW/m}^2$  on the HT rate (a.), the  $\Delta T$  (b.), and the HT coefficient (c.), obtained from using the Woschni correlation. See Table 6 for operating conditions.

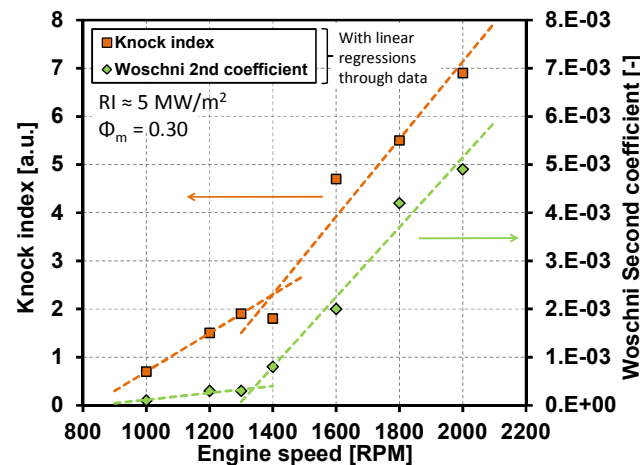


Figure 19: KI and values of the 2<sup>nd</sup> Woschni coefficient (in the combustion-induced velocity term) as a function of engine speed.  $\phi_m = 0.30$  and  $RI \approx 5 \text{ MW/m}^2$ . See Table 6 for the operating conditions.

Finally, these results confirm that, even though the RI correlation includes an engine speed scaling factor using the time-based PPRR instead of the CA-based PPRR (Equation 3), it is not sufficient to account for the actual engine speed effect on the knock propensity (assumptions for that discrepancy were proposed in ref. [20]).

Figure 20 shows that the trend in Exh-L is well reproduced when the effect of the  $\eta_{\text{comb}}$ ,  $\gamma$ , HT and expansion ratio are added up (in this order), with a remainder of less than 0.5%-units. The decrease in the  $\eta_{\text{comb}}$  and the better  $\gamma$  act to reduce the Exh-L. However, the initial decrease in the HT and the lower effective expansion ratio act to increase the Exh-L. Note that the specific trend in Exh-L (reversal trend at  $\sim 1300$  RPM) is strongly influenced by the trend in HT. It is also interesting to notice that, the expansion efficiency does not change significantly since the effect of the more retarded CA50 on the expansion ratio seems to be in a large extent counter-balanced by a better  $\gamma$ .

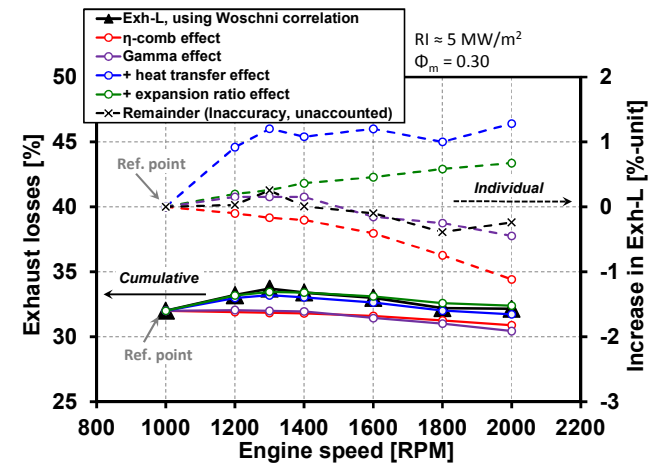


Figure 20: Detailed effect of engine speed on the Exh-L interpolated at  $\phi_m = 0.30$  and for  $RI \approx 5 \text{ MW/m}^2$ . Individual and cumulated contributions of  $\eta_{\text{comb}}$ , HT, CA50 and  $\gamma$  are shown from a reference point. See Table 6 for operating conditions.

### Summary of the Effect of Engine Speed on the $\eta_{\text{th}}$

The peak  $\eta_{\text{th}}$  is achieved for intermediate speeds and maintained, without further optimization, over a relatively wide range, 1200 to 1600 RPM. For a boost pressure of 2.4 bar abs. with  $T_{\text{in}} = 40^\circ\text{C}$  and adjusting CA50 to keep the RI at  $5 \text{ MW/m}^2$ , at constant  $\phi_m = 0.30$ :

- As the engine speed is decreased from 1200 RPM, more time is available for HT which causes the  $\eta_{\text{th}}$  to decrease. This enhancement in the HT exceeds the slightly improved  $\eta_{\text{comb}}$  and slightly higher expansion ratio (minimal effect as CA50 is close to  $366^\circ\text{CA}$ ).
- Between 1200 to 1600 RPM, the  $\eta_{\text{th}}$  is nearly flat. Although it is rather difficult to pin down the exact reason for this behavior, it is likely to be explained by a tradeoff between: a better  $\gamma$  that compensates for both, the initial slow decrease in the  $\eta_{\text{comb}}$  and in the expansion ratio.
- As speed is increased above 1600 RPM, the  $\eta_{\text{th}}$  also decreases because of the drop in the  $\eta_{\text{comb}}$ . The expansion efficiency does not impact significantly the  $\eta_{\text{th}}$ . This is because of the higher  $\gamma$  with increased speed which counter-balances the lower effective

expansion ratio due to CA50 being more retarded. HT was also constant for speeds above 1300 RPM. This is because the reduced time for HT with increased speed is canceled by the increase in the HT-coefficient caused by an increase in the magnitude of the acoustic oscillations.

In addition to ref. [20], these results provide further evidence that the RI correlation does not properly account for the effect of large changes in engine speed on the intensity of the acoustic oscillations. Further work would be needed to assess the importance of this discrepancy and if necessary, to develop a correction to the RI to account for it.

Finally, these results highlight the fact that there is a potential for improvement of the  $\eta_{th}$  at engine speeds above 1200 RPM through an improvement in  $\eta_{comb}$  and by developing methods to advance CA50 without knock.

## Summary & Conclusions

This study was motivated by the need for a detailed understanding of the causes of variations in the gross-indicated- $\eta_{th}$  with operating conditions for HCCI-like, LTGC combustion. To accomplish this, four key parameters, CA50,  $\phi_m$ ,  $T_{in}$ , and engine speed, were independently varied over a large portion of their respective operating ranges. Then, for each parameter sweep, the data were analyzed to determine how the supplied fuel energy was distributed in terms of the work produced ( $\eta_{th}$ ), and the energy lost through 1) incomplete combustion ( $\eta_{comb}$ ), 2) heat transfer (HT) and 3) exhaust enthalpy (Exh-L). Further analysis was conducted to determine the magnitudes of the four main components of the Ext-L:  $\eta_{comb}$ , HT, CA50 and  $\gamma$ .

### Methodology to determine the HT and Exh-L

1. Examination of four methodologies for computing HT and Ext-L showed that using the original Woschni correlation with its two coefficients adjusted for each operating point provided the most sensitive and repeatable model of the HT, and the Exh-L through closure of the energy balance equation.

### Factors affecting the HT

2. With changes in engine operating variables (e.g. CA50,  $\phi_m$  and  $T_{in}$ ) at a given engine speed, the trend in HT can be well explained by the variations in the HT-coefficient, while variations in  $\Delta T$  are less significant.
3. For non-knocking operation, CA50 appears to be a key parameter affecting the HT-coefficient. The HT-coefficient consistently decreased with more retarded CA50, significantly reducing the fraction of fuel energy lost to HT by  $\sim 0.3$  to  $0.5\%$ -units per  $^{\circ}CA$ .
4. The development of strong combustion-induced acoustic oscillations (characteristic of knock) substantially increases the HT-coefficient, with an increase in the slope of the peak  $\Delta HT$ -coefficient/ $\Delta CA50$  during combustion by more than 370%. This causes the HT loss to increase by  $\sim 0.8$  to  $1.2\%$ -units per  $^{\circ}CA$ , as CA50 is advanced beyond the knock-onset point.
5. Increasing the engine speed from 1000 to 2000 RPM enhances the HT-coefficient by  $\sim 25\%$ , due to the increase in the gas

velocity with increased speed. However, for non-knocking operation, the HT decreases because the reduced time for HT with increased speed dominates over the higher HT-coefficient.

### Knock: detection and validity of the RI correlation

6. KI is not a reliable metric for determining the onset of knock. However,  $C_2$ , the scaling coefficient of the combustion-induced velocity term in the Woschni correlation, consistently indicated the onset of knock when adjusted in the manner described in this article.
7. RI of  $\sim 5$  MW/m<sup>2</sup> was confirmed to be a reliable indicator for avoiding knock (and the associated increase in HT) for the sweeps conducted at a constant speed of 1200 RPM.
8. RI was not found to be an effective indicator of knock for large changes in engine speed, supporting the findings in [20].

### Influence of CA50 (at constant $\phi_m$ )

9. For typical LTGC operation with CA50 retarded “well” after TDC to avoid engine knock, it is desirable to advance CA50 as much as possible toward the knock-onset point to maximize the  $\eta_{th}$ . The increase  $\eta_{th}$  results mainly from the increased expansion ratio and to a lesser extent from better  $\eta_{comb}$ .
10. If CA50 is advanced beyond the knock-onset point, the HT substantially increases (see conclusions #3 & 4). For relatively low  $\phi_m$  (with less retarded CA50), this causes an immediate decrease in the  $\eta_{th}$ . For higher  $\phi_m$  (with more retarded CA50), the  $\eta_{th}$  still increases because of the greater benefit of advancing the CA50 when it occurs well after TDC. However, the rate of increase in  $\eta_{th}$  with CA50 advancement is reduced due to the increased HT with knock. Nevertheless, these higher  $\eta_{th}$  points are not considered acceptable due to the excessive noise and potential engine damage over time from knock.

### Influence of $\phi_m$ (at constant RI)

11. Increasing  $\phi_m$  at constant RI, which produces hotter combustion, yields to a significant decrease in the fraction of the energy lost to HT. The lower HT is mainly attributed to a progressive decrease in the HT-coefficient as CA50 is retarded to prevent knock. HT is found to decrease by  $\sim 0.8\%$ -units per  $^{\circ}CA$  as  $\phi_m$  is increased at constant RI.
12. As  $\phi_m$  is increased the  $\eta_{th}$  peaks at an intermediate  $\phi_m$  of  $\sim 0.30$  for our baseline conditions due to a tradeoff between: 1) increased  $\eta_{comb}$  and decreased HT; and 2) decreased expansion efficiency due to more retarded CA50 and a reduced  $\gamma$ . Unlike the effect of varying CA50 alone (at constant  $\phi_m$ ), the decrease in the  $\eta_{th}$  with more CA50 retard as  $\phi_m$  is increased, is not only caused by the lower expansion ratio, but mainly by the lower  $\gamma$ .

### Influence of $T_{in}$ (at constant RI)

13. At 1200 RPM and  $P_{in} = 2.4$  bar abs, reducing  $T_{in}$  improved the peak  $\eta_{th}$  by  $\sim 0.25\%$ -units every  $10^{\circ}C$  decrement until reaching  $T_{in} = 40^{\circ}C$ .  $T_{in}$  of 30 and  $40^{\circ}C$  gave the same maximum  $\eta_{th}$ . Increasing the  $T_{in}$  above  $40^{\circ}C$  reduces the  $\eta_{th}$  because of the decrease in  $\gamma$  as more EGR is needed to control the CA50.

## Influence of RPM (at constant RI)

14. As engine speed is increased, the highest  $\eta_{th}$  was obtained for intermediate engine speeds between 1200 to 1600 RPM due to a tradeoff between: 1) the decrease in the  $\eta_{comb}$  with increase speed, and 2) the increase in the HT as speed is reduced from 1300 RPM.
15. RI correlation was found to not be effective for indicating the onset of knock for changes in engine speed.

## References

1. Reitz, R.D., *Directions in internal combustion engine research*. Combustion and Flame, 2013. 160(1): p. 1-8. doi:10.1016/j.combustflame.2012.11.002.
2. Dec, J.E., *Advanced Compression-Ignition Combustion for High Efficiency and Ultra-Low NOX and Soot*, in *Encyclopedia of Automotive Engineering*, D. D.E.F. Crolla, T. Kobayashi and N. Vaughan (Eds.), John Wiley & Sons Ltd, Editor 2015: Chichester, UK. p. 267-306.
3. Dec, J.E., *Advanced compression-ignition engines—understanding the in-cylinder processes*. Proceedings of the Combustion Institute, 2009. 32(2): p. 2727-2742. doi:10.1016/j.proci.2008.08.008.
4. Dec, J.E., Y. Yang, and N. Dronniou, *Improving Efficiency and Using E10 for Higher Loads in Boosted HCCI Engines*. SAE Int. J. Engines, 2012. 5(3): p. 1009-1032. doi:10.4271/2012-01-1107.
5. Christensen, M., et al., *Supercharged Homogeneous Charge Compression Ignition*. 1998,SAE International, 10.4271/980787.
6. Saxena, S. and I.D. Bedoya, *Fundamental phenomena affecting low temperature combustion and HCCI engines, high load limits and strategies for extending these limits*. Progress in Energy and Combustion Science, 2013. 39(5): p. 457-488. doi: 10.1016/j.peccs.2013.05.002.
7. Sjöberg, M. and J.E. Dec, *An investigation into lowest acceptable combustion temperatures for hydrocarbon fuels in HCCI engines*. Proceedings of the Combustion Institute, 2005. 30(2): p. 2719-2726. doi: 10.1016/j.proci.2004.08.132.
8. Dec, J.E. and M. Sjöberg, *A Parametric Study of HCCI Combustion - the Sources of Emissions at Low Loads and the Effects of GDI Fuel Injection*. 2003,SAE International, doi:10.4271/2003-01-0752.
9. Sjöberg, M. and J.E. Dec, *Combined Effects of Fuel-Type and Engine Speed on Intake Temperature Requirements and Completeness of Bulk-Gas Reactions for HCCI Combustion*. 2003,SAE International, 10.4271/2003-01-3173.
10. Dec, J.E., *A Computational Study of the Effects of Low Fuel Loading and EGR on Heat Release Rates and Combustion Limits in HCCI Engines*. 2002,SAE International, 10.4271/2002-01-1309.
11. Christensen, M., B. Johansson, and A. Hultqvist, *The Effect of Piston Topland Geometry on Emissions of Unburned Hydrocarbons from a Homogeneous Charge Compression Ignition (HCCI) Engine*. 2001,SAE International, 10.4271/2001-01-1893.
12. Aceves, S.M., et al., *Piston-Liner Crevice Geometry Effect on HCCI Combustion by Multi-Zone Analysis*. 2002,SAE International, 10.4271/2002-01-2869.
13. Dec, J.E. and Y. Yang, *Boosted HCCI for High Power without Engine Knock and with Ultra-Low NOx Emissions - using Conventional Gasoline*. SAE Int. J. Engines, 2010. 3(1): p. 750-767. doi:10.4271/2010-01-1086.
14. Dec, J.E., Y. Yang, and N. Dronniou, *Boosted HCCI - Controlling Pressure-Rise Rates for Performance Improvements using Partial Fuel Stratification with Conventional Gasoline*. SAE Int. J. Engines, 2011. 4(1): p. 1169-1189. doi:10.4271/2011-01-0897.
15. Saxena, S., et al., *Understanding Loss Mechanisms and Identifying Areas of Improvement for HCCI Engines Using Detailed Exergy Analysis*. Journal of Engineering for Gas Turbines and Power, 2013. 135(9): p. 091505-091505. 10.1115/1.4024589.
16. Saxena, S., et al., *Understanding optimal engine operating strategies for gasoline-fueled HCCI engines using crank-angle resolved exergy analysis*. Applied Energy, 2014. 114(0): p. 155-163. doi: 10.1016/j.apenergy.2013.09.056.
17. Sjöberg, M., J.E. Dec, and N.P. Cernansky, *Potential of Thermal Stratification and Combustion Retard for Reducing Pressure-Rise Rates in HCCI Engines, Based on Multi-Zone Modeling and Experiments*. 2005,SAE International, doi:10.4271/2005-01-0113.
18. Tsurushima, T., et al., *The Effect of Knock on Heat Loss in Homogeneous Charge Compression Ignition Engines*. 2002,SAE International, doi:10.4271/2002-01-0108.
19. Winkler, N., *Effect of pressure oscillations on in-cylinder heat transfer – through large eddy simulation*. International Journal of Engine Research, 2014. 10.1177/1468087414544899.
20. Dernote, J., J. Dec, and C. Ji, *Investigation of the Sources of Combustion Noise in HCCI Engines*. SAE Int. J. Engines, 2014. 7(2): p. 730-761. 10.4271/2014-01-1272.
21. Eng, J.A., *Characterization of Pressure Waves in HCCI Combustion*. 2002,SAE International, doi:10.4271/2002-01-2859.
22. Kodavasal, J., et al., *The effect of diluent composition on homogeneous charge compression ignition auto-ignition and combustion duration*. Proceedings of the Combustion Institute, (0). <http://dx.doi.org/10.1016/j.proci.2014.06.152>.
23. Heywood, J.B., *Internal Combustion Engine Fundamentals*, 1988, New York: McGraw-Hill.
24. Chang, J., et al., *New Heat Transfer Correlation for an HCCI Engine Derived from Measurements of Instantaneous Surface Heat Flux*. 2004,SAE International, 10.4271/2004-01-2996.
25. Woschni, G., *A Universally Applicable Equation for the Instantaneous Heat Transfer Coefficient in the Internal Combustion Engine*. SAE Int. J. Engines, 1967
26. Annand, W.J.D. and T.H. Ma, *Instantaneous heat transfer rates to the cylinder head surface of a small compression-ignition engine*. Proc. Instn mech. Engrs, 1970-71. 185(72 71): p. 976-987
27. Hohenberg, G.F., *Advanced Approaches for Heat Transfer Calculations*. SAE Technical Paper, 1979. 10.4271/790825.
28. Borman, G. and K. Nishiwaki, *Internal-combustion engine heat transfer*. Progress in Energy and Combustion Science, 1987. 13(1): p. 1-46. doi.org/10.1016/0360-1285(87)90005-0.
29. Goldsborough, S.S., *Evaluating the Heat Losses from HCCI Combustion within a Rapid Compression Expansion Machine*. 2006,SAE International, 10.4271/2006-01-0870.
30. Hensel, S., et al., *A New Model to Describe the Heat Transfer in HCCI Gasoline Engines*. SAE Int. J. Engines, 2009. 2(1): p. 33-47. 10.4271/2009-01-0129.

31. Soyhan, H.S., et al., *Evaluation of heat transfer correlations for HCCI engine modeling*. Applied Thermal Engineering, 2009. 29(2–3): p. 541-549. doi: 10.1016/j.applthermaleng.2008.03.014.
32. Sjöberg, M. and J.E. Dec, *An Investigation of the Relationship Between Measured Intake Temperature, BDC Temperature, and Combustion Phasing for Premixed and DI HCCI Engines*. 2004,SAE International, 10.4271/2004-01-1900.
33. Vressner, A., et al., *Pressure Oscillations During Rapid HCCI Combustion*. 2003,SAE International 2003-01-3217, doi:10.4271/2003-01-3217.
34. Dahl, D., M. Andersson, and I. Denbratt, *The Origin of Pressure Waves in High Load HCCI Combustion: A High-Speed Video Analysis*. Combustion Science and Technology, 2011. 183(11): p. 1266-1281. doi:10.1080/00102202.2011.589875.
35. Grandin, B. and I. Denbratt, *The Effect of Knock on Heat Transfer in SI Engines*. 2002,SAE International, 10.4271/2002-01-0238.
36. Dec, J.E. and M. Sjöberg, *Isolating the Effects of Fuel Chemistry on Combustion Phasing in an HCCI Engine and the Potential of Fuel Stratification for Ignition Control*. 2004,SAE International, 10.4271/2004-01-0557.
37. Sjöberg, M. and J.E. Dec, *Comparing late-cycle autoignition stability for single- and two-stage ignition fuels in HCCI engines*. Proceedings of the Combustion Institute, 2007. 31(2): p. 2895-2902. doi:10.1016/j.proci.2006.08.010.
38. Aceves, S.M., et al., *Spatial Analysis of Emissions Sources for HCCI Combustion at Low Loads Using a Multi-Zone Model*. 2004,SAE International, 10.4271/2004-01-1910.
39. Ji, C., et al., *Effect of Ignition Improvers on the Combustion Performance of Regular-Grade E10 Gasoline in an HCCI Engine*. SAE Int. J. Engines, 2014. 7(2): p. 790-806. 10.4271/2014-01-1282.

## Contact Information

Corresponding authors: Jeremie Derron and John Dec, Sandia National Laboratories, MS-9053, P.O. Box 969, Livermore, CA 94551-0969, USA.

## Acknowledgments

The authors would like to thank Kenneth St. Hilaire, Christopher Carlen, David Cicone, Alberto Garcia and Gary Hubbard of Sandia National Laboratories for their dedicated support of the HCCI Engine Laboratory. The authors would also like to thank Yi Yang (now at University of Melbourne, Australia) for his help in acquiring some of the datasets used in this study (CA50 effect). Furthermore, the authors wish to acknowledge Brian Peterson and Ethan Eagle (both working at Sandia National Laboratories) for reviewing this article and their valuable comments and suggestions.

This work was performed at the Combustion Research Facility, Sandia National Laboratories, Livermore, CA, Support was provided by the U.S. Department of Energy, Office of Vehicle Technologies. Sandia is a multiprogram laboratory operated by the Sandia Corporation, a Lockheed Martin Company, for the United States Department of Energy's National Nuclear Security Administration under contract DE-AC04-94AL85000.

## Definitions/Abbreviations

$\gamma$	Ratio of specific heats = $c_p/c_v$
$\Delta T$	$T_{\text{gas}} - T_{\text{wall}}$
$\eta_{\text{comb}}, \eta_{\text{th}}$	Combustion and thermal efficiencies
$\phi, \phi_m$	Air-based equivalence ratio and charge-mass equivalence ratio
<b>AHRR</b>	Apparent Heat Release Rate
<b>a.u.</b>	Arbitrary Unit
<b>B</b>	Cylinder Bore
$C_2$	Coefficient of the combustion-induced gas velocity term in the Woschni correlation
<b>CNL</b>	Combustion Noise Level
<b>CR</b>	Compression Ratio
<b>Exh-L</b>	Exhaust Losses
<b>GDI</b>	Gasoline-type Direct Injector
<b>HT</b>	Heat Transfer
<b>KI</b>	Knock Index
<b>LHV</b>	Lower Heating of Value
<b>LTGC</b>	Low-Temperature Gasoline Combustion
<b>LTHR</b>	Low-Temperature Heat Release
<b>MON</b>	Motor Octane Number
$P_{\text{max}}$	Maximum cycle pressure
<b>PM</b>	PreMixed
<b>PRR, PPRR</b>	Pressure Rise Rate and Peak PRR
<b>RI</b>	Ringing Intensity
<b>RON</b>	Research Octane Number
<b>RPM</b>	Rotations Per Minute
<b>SOI</b>	Start Of Injection
$T_{\text{gas}}, T_{\text{max}}$	Mass-average and maximum mass-average charge temperature
<b>TDC</b>	Top Dead Center

## Appendix 1 – CA50 as a Fundamental Parameter Driving the HT

Different scenarios of CA50 sweeps at 1200 RPM and how they affect the HT are presented in Figure 21. HT was determined using the Woschni analysis. These different sweeps are briefly introduced below.

1. The green colored data in Figure 21 show the two CA50 sweeps ( $\phi_m = 0.32$  and  $0.42$ ) from the first part of the results section (Figure 8). For each sweep,  $\phi_m$  was held constant while CA50 was advanced by reducing the amount of EGR, which led to an increase in the RI (Figure 7). The knock onset points matching an  $RI \approx 5 \text{ MW/m}^2$  is indicated by the “star” symbols in Figure 21. Of interest here, with more advanced CA50, the peak  $\Delta T$  (Figure 9b) and the HT-coefficient increase (Figure 7 and Figure 9).
2. The group of curves at the bottom - left of the figure show the  $\phi_m$  / CA50 sweeps at constant  $RI \approx 5 \text{ MW/m}^2$  for different  $T_{in}$ , from Figure 11c and Figure 14c, replotted here as a function of CA50. With increasing  $\phi_m$ , the peak  $\Delta T$  increases (Figure 12b) and the HT-coefficient decreases (Figure 12c). In addition, these curves show the good repeatability of HT analysis. Both  $\phi_m$  / CA50 sweeps at  $T_{in} = 30^\circ\text{C}$  from Figure 11c and Figure 14c overlap (as well as for the higher  $T_{in}$ ) within +/- 0.5%-units.
3. Shown in blue in Figure 21 is another  $\phi_m$  / CA50 sweep (not presented in the core of the article) for which  $\phi_m$  was increased while allowing the CA50 to vary (at constant  $T_{in}$  and with no EGR). Therefore, in contrast to the  $\phi_m$  / CA50 sweeps at  $RI \approx 5 \text{ MW/m}^2$  (scenario 2), as  $\phi_m$  increases, the CA50 becomes more advanced and the RI increases. For  $RI > 5 \text{ MW/m}^2$ , a change of slope in the HT is also perceptible, indicating the onset of knock (highlighted with a “star” symbol). For this case, both the peak  $\Delta T$  and the HT-coefficient increase with more advanced CA50. For more information about this sweep, refer to refs. [4] and [20].

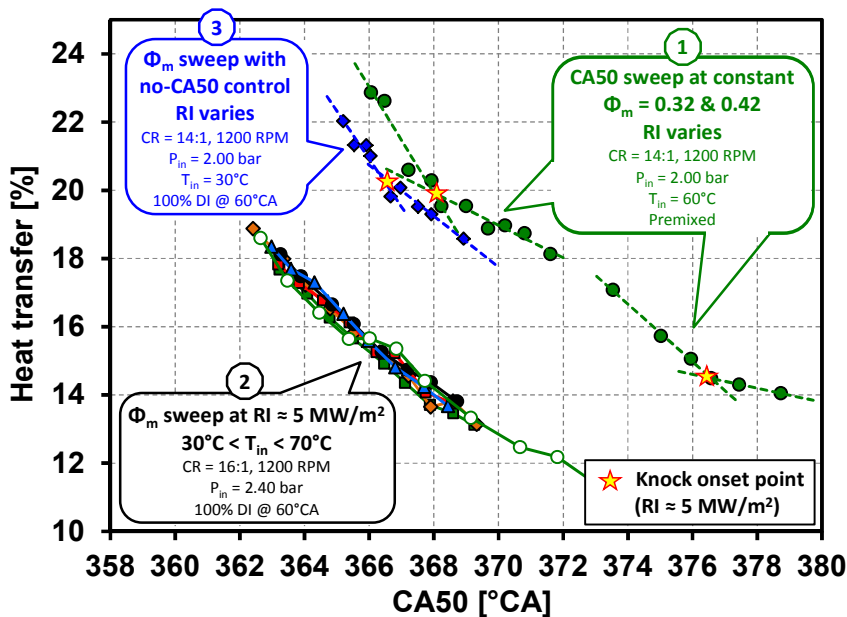


Figure 21: HT from Woschni analysis as a function of CA50 for different scenarios.

A comparison between these datasets will not be broached because too many parameters are varying simultaneously (*i.e.* CR,  $P_{in}$ , fuelling strategy and type of gasoline).

Instead, the key point to notice from Figure 21 is that the HT consistently decreases with more retarded CA50. This is somewhat expected for scenarios 1 and 3, since the peak- $\Delta T$  decreases with more retarded CA50. However, this is not as straightforward for the sweeps of scenario 2 since  $\Delta T$  increases because  $\phi_m$  is increased while CA50 is being more retarded (refer to the discussion in conjunction with Figure 12). The fact that HT consistently decreases with CA50 was also mentioned by Saxena *et al.* [16].

The decrease in the HT with CA50 retard consistently better correlates with a decrease in the HT-coefficient than the  $\Delta T$ . This indicates that the HT-coefficient is the dominant factor driving the HT. Moreover, the HT-coefficient seems to be strongly affected by the phasing of the combustion (*i.e.* CA50). In other words, this observation suggests that, with more CA50 retard, the intensity of the turbulent eddies near the wall or other in-cylinder flows that drive the HT vary more than the changes in the thermal state ( $\Delta T$ ). Additional / fundamental investigations would be required to better understand this phenomenon.

## Appendix 2 – Incremental Changes in Exh-L due to Variations in $\eta_{\text{comb}}$ and HT

The incremental changes in the Exh-L due to variations in  $\eta_{\text{comb}}$  and HT are approximated as follows, starting from a reference point for which  $i = 0$ . For example, this reference point is chosen to be the most retarded point for the CA50 sweeps in Figure 10. The values to be inserted in the equations below are directly read from figures like Figure 8. These equations are established as follows: for Equation 15, the variation in Exh-L due to variation in  $\eta_{\text{comb}}$  between points  $(i-1)$  and  $(i)$  is defined by the variation of the mean fraction, between these two points, of burned fuel that goes into the exhaust. Note that combustion inefficiency (*i.e.*  $= 100 - \eta_{\text{comb}}$ ) is not included in the denominator because, obviously, no fraction of the change in  $\eta_{\text{comb}}$  goes back to the combustion inefficiency. A change in  $\eta_{\text{comb}}$  only affects the  $\eta_{\text{th}}$ , the Exh-L and the HT. The same procedure is used to determine the variations in Exh-L due to changes in the HT (Equation 16), except that changes in HT only affect the  $\eta_{\text{th}}$  and the Exh-L as shown in the denominator of Equation 16. For good accuracy in using these equations, relatively fine resolution in the data is needed.

$$\begin{aligned} &\text{Incremental change in Exh-L due to variation in } \eta_{\text{comb}} (i) = \\ &\quad \text{Fraction of energy lost into exhaust} \\ &\quad \underbrace{(\eta_{\text{comb}}(i) - \eta_{\text{comb}}(i-1))}_{\text{Change in } \eta_{\text{comb}}} \times \underbrace{\frac{\overbrace{\text{ExhL}(i) + \text{ExhL}(i-1)}}{\text{ExhL}(i) + \text{ExhL}(i-1) + \text{HT}(i) + \text{HT}(i-1) + \eta_{\text{th}}(i) + \eta_{\text{th}}(i-1)}}_{\text{Fraction of the energy pathways affected by a change in } \eta_{\text{comb}}} \end{aligned} \quad (15)$$

$$\begin{aligned} &\text{Incremental change in Exh-L due to variation in HT } (i) = \\ &\quad \text{Fraction of energy lost into exhaust} \\ &\quad \underbrace{(\text{HT}(i) - \text{HT}(i-1))}_{\text{Change in HT}} \times \underbrace{\frac{\overbrace{\text{ExhL}(i) + \text{ExhL}(i-1)}}{\text{ExhL}(i) + \text{ExhL}(i-1) + \eta_{\text{th}}(i) + \eta_{\text{th}}(i-1)}}_{\text{Fraction of the energy pathways affected by a change in HT}} \end{aligned} \quad (16)$$

## Appendix 3 – Influence of $T_{\text{in}}$ / Limitation of the $\eta_{\text{th}}$ between 30 and 40°C

For a constant  $\phi_{\text{m}}$  of 0.30 for instance, decreasing  $T_{\text{in}}$  from 40°C to 30°C does not provide any gain in  $\eta_{\text{th}}$  (Figure 14a). The decrease in  $\eta_{\text{comb}}$  with the reduced  $T_{\text{in}}$  is one factor for this limitation, but the difference in  $\eta_{\text{comb}}$  is too small to compensate for: 1) the slightly more advanced CA50 for  $T_{\text{in}} = 30^\circ\text{C}$ , which provides a slightly better expansion ratio and 2) the higher value of  $\gamma$  for  $T_{\text{in}} = 30^\circ\text{C}$ .

The main reason for this limitation in the  $\eta_{\text{th}}$  improvement with reduced  $T_{\text{in}}$  is related to the greater increase in the HT during combustion when  $T_{\text{in}}$  is decreased from 40 to 30°C, as shown in Figure 15a. This abrupt increase in the HT appears to correlate well with the more advanced CA50 at  $T_{\text{in}} = 30^\circ\text{C}$ . However, as demonstrated in the first part of the results section (CA50 effect), this slightly more advanced CA50 should provide more gain in expansion efficiency than the increase in the HT, particularly at higher- $\phi_{\text{m}}$ , if the engine is not knocking. In our experiments, knock is believed to be reasonably avoided if the RI is kept below  $\sim 5 \text{ MW/m}^2$ , which was applied for these tests. However, it is believed that small acoustic oscillations (light knock or borderline knock) occur for these 30°C data and this is the reason for the larger increase in the HT from 40 to 30°C observed in Figure 15a. This explanation is supported by the faster increase in the HT-coefficient from 40 to 30°C as seen in Figure 15c.

Figure 22 further supports the hypothesis that for  $T_{\text{in}} = 30^\circ\text{C}$ , the knock intensity is slightly higher than for the other  $T_{\text{in}}$ . First, the RI is generally slightly higher for this dataset, and it is a little above  $5 \text{ MW/m}^2$ . Also, the values of the KI and  $C_2$  are significantly and consistently higher for the 30°C  $\phi_{\text{m}}$ -sweep, again suggesting that light-knock is occurring. Take together these differences for the 30°C sweep in Figure 22 and the sudden rise of the HT-rate during the combustion event in Figure 15c, indicate that light knock is the most probable cause for the increased heat transfer at  $T_{\text{in}} = 30^\circ\text{C}$ . Thus, with a slightly more advanced-CA50 for  $T_{\text{in}} = 30^\circ\text{C}$  compared to 40°C (Figure 14a), the increase in HT due to light knock in combination with the reduced  $\eta_{\text{comb}}$  with reduced  $T_{\text{in}}$ , appear to be sufficient to dominate the slight improvement in the expansion ratio and the better  $\gamma$ . The net effect being that  $\eta_{\text{th}}$  does not increase from 40 to 30°C.

It should be noted that the RI for  $T_{\text{in}} = 30^\circ\text{C}$ , generally slightly higher than  $5 \text{ MW/m}^2$ , does not seem to be enough to explain that the magnitude of the acoustic oscillations is slightly higher for this  $T_{\text{in}} = 30^\circ\text{C}$  sweep. To fully understand the reasons for this behavior further work would be needed. However, it can be noticed in Figure 22, that the RI for the sweeps at  $T_{\text{in}} = 40^\circ\text{C}$  and  $50^\circ\text{C}$  came out to be closer to  $4.6$  than  $5.0 \text{ MW/m}^2$ , whereas the RI for the  $T_{\text{in}} = 60^\circ\text{C}$  and  $70^\circ\text{C}$  sweeps is very close to  $5.0 \text{ MW/m}^2$ . This suggests that the KI and  $C_2$  are perhaps slightly undervalued for  $T_{\text{in}} = 40^\circ\text{C}$  and  $50^\circ\text{C}$ , while those for  $T_{\text{in}} = 60^\circ\text{C}$  and  $70^\circ\text{C}$  are correct. If RI was successfully kept exactly at  $5 \text{ MW/m}^2$  for all  $T_{\text{in}}$ s, the KI and  $C_2$  curves for  $T_{\text{in}} = 40^\circ\text{C}$  and  $50^\circ\text{C}$  should shift upward so they fall between the current  $T_{\text{in}} = 60^\circ\text{C}$  and  $T_{\text{in}} = 30^\circ\text{C}$  curves. Thus, they might show a progressive increase as  $T_{\text{in}}$  is reduced. If this is the case, it suggests a potential very small inaccuracy of the RI correlation as  $T_{\text{in}}$  is varied. However, this effect would be very small and any discrepancy is not expected to induce any significant change to the observed trend of  $\eta_{\text{th}}$  vs.  $T_{\text{in}}$  presented in this work. It is considered that this error falls within the accuracy limits of both the RI correlation and the experimental measurements, which already enable explanations for variations of 0.1 to 0.2% of the  $\eta_{\text{th}}$ .

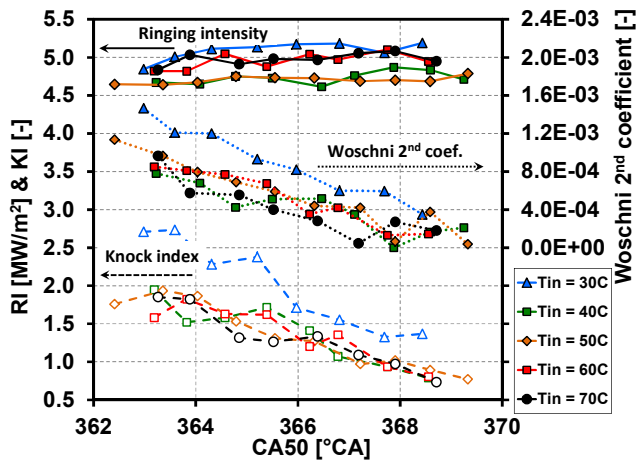


Figure 22: RI, KI and values of the 2<sup>nd</sup> Woschni coefficient (in the combustion-induced velocity term) as a function of CA50 (more retarded as  $\phi_m$  increases) for several  $T_{in}$ . See for Table 5 operating conditions.

#### Appendix 4 – Influence of Engine Speed on the Energy Distribution

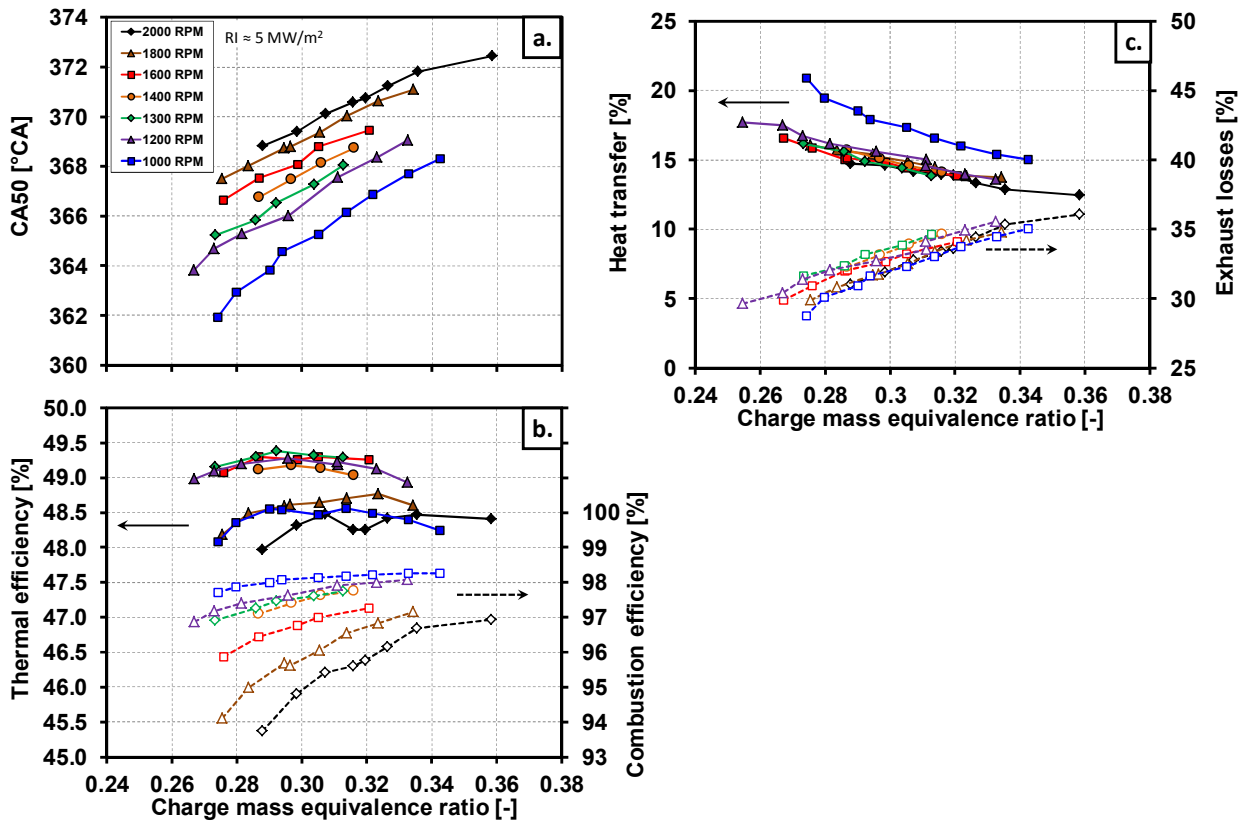


Figure 23: Variation of CA50 (a.) and energy distribution for  $\phi_m$  sweeps at different RPM and  $Ri \approx 5 \text{ MW/m}^2$ ; (b.):  $\eta_{th}$  and  $\eta_{comb}$ . (c.): HT and Exh-L derived from the use of the Woschni correlation. See Table 6 for operating conditions.